JAAS

Accepted Manuscript

This is an *Accepted Manuscript*, which has been through the Royal Society of Chemistry peer review process and has been accepted for publication.

Accepted Manuscripts are published online shortly after acceptance, before technical editing, formatting and proof reading. Using this free service, authors can make their results available to the community, in citable form, before we publish the edited article. We will replace this *Accepted Manuscript* with the edited and formatted *Advance Article* as soon as it is available.

You can find more information about *Accepted Manuscripts* in the Information for Authors.

Please note that technical editing may introduce minor changes to the text and/or graphics, which may alter content. The journal's standard Terms & Conditions and the Ethical guidelines still apply. In no event shall the Royal Society of Chemistry be held responsible for any errors or omissions in this *Accepted Manuscript* or any consequences arising from the use of any information it contains.

ROYAL SOCIETY OF CHEMISTRY

www.rsc.org/jaas

Capabilities of sequential and quasi-simultaneous LA-ICPMS for the multi-element analysis of small quantity of liquids (pl to nl): insights from fluid inclusion analysis

Matthieu Harlaux[1], Olga Borovinskaya[2,3], Daniel A. Frick[2,4], Daniel Tabersky[2], Sabrina Gschwind[2], Antonin Richard[1], Detlef Günther[2] and Julien Mercadier[1*]

1: Université de Lorraine, CNRS, CREGU, GeoRessources, F-54506 Vandœuvre-lès-Nancy, France.
2: ETH Zurich, Department of Chemistry and Applied Biosciences, Laboratory of Inorganic Chemistry, Vladimir-Prelog-Weg 1, CH-8093 Zürich, Switzerland.
3: Present address: Tofwerk AG, Uttigenstrasse 22, CH-3600 Thun, Switzerland.
4: Present address: GFZ German Research Centre for Geosciences, Section 3.4 Earth Surface Geochemistry, Telegrafenberg, D-14473 Potsdam, Germany.
* Corresponding author: julien.mercadier@univ-lorraine.fr

Abstract

Three configurations of inductively coupled plasma mass spectrometers (ICPMS), namely: a quadrupole (QMS) and a sector-field (SFMS), both equipped with a standard cylindrical ablation cell, and an orthogonal time-of-flight (TOFMS), equipped with a fast washout ablation cell, were coupled with the same 193 nm Excimer laser ablation system in order to evaluate their capabilities for measurement of multiple minor and trace elements in small quantities of liquids (pl to nl), such as fluid inclusions. Analyses were performed with different objects: (i) multi-element solutions sealed in silica capillaries of internal diameter of 20 µm serving as synthetic analogues of natural fluid inclusions; (ii) natural two-phase (liquid + vapour) fluid inclusions with low salinity (ca. 4.8 wt% NaCl eq) and homogeneous compositions, trapped in quartz crystals from the Alps; (iii) natural multi-phase (liquid + vapour + multiple solids) fluid inclusions with high salinity (ca. 13-15 wt% NaCl eq) and homogeneous compositions, trapped in quartz crystals from the Zambian Copperbelt. This study demonstrates that the SFMS and TOFMS provide improvements, particularly in term of limits of detection (LODs) and precision, compared to the QMS traditionally used for the measurement of fluid inclusions. SFMS leads on average to lower LODs within one order of

magnitude compared to QMS and TOFMS, but precision and accuracy are lower due to longer acquisition cycle times. TOFMS presents both advantages of having rapid and quasi-simultaneous acquisition for all isotopes from ^{6}Li to ^{238}U in a very short cycle time down to 30 µs, with higher precisions and lower LODs than for QMS for isotopes with m/Q > 11. Its use, coupled to a fast washout cell, leads to (i) the improvement in the analysis of small-size (< 10 µm) and multi-phase fluid inclusions and (ii) detection of higher number of isotopes compared to QMS and SFMS, which are both limited by the number of measured isotopes from short transient signals of fluid inclusions. Consequently, the tested TOFMS, coupled with a fast washout ablation cell, appears to be a promising instrument for the analysis of natural fluid inclusions by LA-ICPMS, especially for small, multi-phase and/or low salinity fluid inclusions.

1. Introduction

The multi-element quantification of minor and trace elements, typically present in concentrations from the ng l^{-1} to g l^{-1} range, in small quantities of liquids (pl to nl) is of a major analytical interest for a large variety of applied fields, for instance in chemistry[1,2], geology[3-8], biology[9], medicine[10,11], climatology[12] or environmental sciences[13]. One current analytical challenge is to improve and to develop strategies for analyses of such small quantities of liquid, whether by: (1) reducing the detectable fluid volume; (2) increasing the number of detectable elements; (3) increasing the sensitivity of the instruments and/or (4) increasing the precision and accuracy of the measurements. For example, a recent research field has been developed on the detection and quantification of nanoparticles carried by liquid microdroplets, in order to study the risks of nanoparticles for the environment and the human health.[1,14] Such microdroplets have a typical diameter of 30-40 µm and generate very short transient signals when analysed by inductively coupled mass spectrometry, and remain a challenging analytical issue.[1,14]

One of the most challenging case studies are the geological fluids trapped in natural fluid inclusions. The latter represent droplets of fluids, ranging from pl to nl in volume, and trapped in tiny cavities of typically tens of µm in diameter during the crystallization of minerals. Natural fluid inclusions can consequently provide direct information about the composition of fluids from which minerals have precipitated and represent therefore invaluable tool for the reconstruction of the geological fluids, which have circulated in the Earth's interior for ca. 4.6

billions years[15]. They are of primary interest for a large set of geological research fields, in particular for the study of diagenesis[16], metamorphism[17,18], geothermal systems[19,20], oil and gas deposits[21,22] and mineral deposits[23-26]. Natural geological fluids are characterized by an extremely wide variety of chemical elements, potentially from Li to U, with varying concentration ranges from percent to below μg g^{-1}, and their analysis represents consequently high analytical challenge.

Due to its high sensitivity, speed and multi-element capabilities, laser ablation coupled to inductively coupled plasma quadrupole mass spectrometers (LA-ICPQMS, hereafter called QMS) has proven[27] to be one of the most suitable techniques for the analysis of geological fluids trapped in natural crystals (see review in Pettke *et al.*[6]). This technique offers several advantages compared to other instrumentations (LIBS, synchrotron-XRF or PIXE for example), like well-controlled ablation of quartz using UV lasers[28], the large concentration dynamic range (10^9 to 10^{11}), the relatively low limits of detection (down to 0.01 μg g^{-1})[6] and fast acquisition times (in the ms range per isotope). At the present time, sequential scanning QMS typically allows registering 20 isotope signals with m/Q from 7 to 238 in less than 260 ms in a single mass scan.[6] The development of specific quantification strategies to evaluate the elemental concentrations by QMS was also a major cause of the increasing acceptance of LA-ICPMS in fluid inclusion research.[3-5,29-30]

The signals generated in QMS from this type of tiny samples are usually of relatively low intensity for minor to trace elements and last only for several seconds due to the rapid release of the fluid during the ablation process.[28] Unambiguous multi-element detection of such transient signals is not a trivial task when sequential quadrupole mass spectrometers are used and often requires a compromise between the signal duration, acquisition parameters of the mass spectrometer and the number of isotopes to be monitored.[4-6,31] The current use of QMS is consequently restricted to relatively large-size (> 30 μm) and moderate- to high-salinity (> 5 wt% NaCl eq) fluid inclusions, which contain detectable concentrations of the analytes.[4-6] However, this type of fluid inclusions represents a rather limited proportion of the fluid inclusions present in natural samples and are potentially more affected by post-crystallization modifications (*e.g.* leaking, cracks and/or deformation) than smaller ones. Moreover, even for such samples, the number of isotopes that can be monitored rarely exceeds 20, including majors, minors and trace elements. This can consequently makes a global and representative understanding of the chemical composition of paleofluids difficult. Furthermore, analytical limitations are encountered for small-size (< 10 μm) fluid inclusions as well as for those

containing low trace element contents (< 1 μg g^{-1}), thus constraining the interpretation of several geological processes related to paleofluids circulations.

Other types of mass spectrometers coupled to laser ablation systems have been tested during the last years, with the aim of improving the quantification of elemental and even isotopic compositions of geological fluids (see review of Pettke *et al.*[6]). Single-collector sector-field mass spectrometers coupled to laser ablation (LA-ICPSFMS, hereafter called SFMS) have achieved about ten times higher sensitivities compared to QMS instrumentation for natural fluid inclusions.[31] However, QMS and SFMS are both limited by sequential detection, which can deteriorate accuracy and precision of the analysis due to signal aliasing.[14,32] Moreover, SFMS are also limited by the multiple magnet jumps required to cover the entire mass range from Li to U, which results in longer cycle times compared to QMS, with around 20% longer cycle for 20 isotopes measured. This temporal limitation could appear as a main drawback especially for small fluid inclusions (< 20 μm), but the recent study by Wälle and Heinrich[31] concluded that SF expands the accessible fluid inclusion size range to 2 or 3 times smaller volumes or 10 times lower concentrations in larger inclusions.

One application of multi-collector mass spectrometers coupled to laser ablation (LA-MC-ICPMS) was recently successfully proposed for the determination of Pb isotopic ratios in natural fluid inclusions.[33] However, the small volume of fluid trapped is a major limitation for the precise measurement of isotopic ratios. Even with a multi-collection and high sensitivity, the extremely limited duration of the signal and the relatively low concentration allow successful results only for exceptional geological conditions, for example for the Bingham Cu-Mo-Au deposit.[34] Even if LA-MC-ICPMS present far lower limits of detection than QMS, they do not allow the acquisition of the whole mass spectra, which is a strong limitation for fluid inclusion studies, especially with the need to measure an internal standard (mainly ^{23}Na) for the quantification of the fluid compositions.[4]

Detection based on time-of-flight mass spectrometers coupled to laser ablation (LA-ICPTOFMS, hereafter called TOFMS) has been considered highly promising for multi-element analysis of very short transient signals, because it allows quasi-simultaneous measurements of all isotopes.[35] This configuration of a mass spectrometer allows overcoming the problem of aliasing for short transient signals and could consequently improve the quantification of fluids trapped in natural minerals.[14,36,37] First generations of TOFMS with an axial configuration applied to natural fluid inclusions had lower sensitivities, low signal to noise ratio, low dynamic range and higher limits of detection compared to QMS.[4,39] Nevertheless, previous study on multiphase fluid inclusions from the Mole granite[38]

demonstrated the abilities of axial TOFMS for the detection of up to 42 isotopes above the LODs, as well as the discrimination of signals of elements contained in fluid or in solid matrices. Recently, a new prototype of TOFMS with an orthogonal configuration has been developed[14,36], which allows quasi-simultaneous detection of the whole mass range, with a high temporal resolution of 30 µs, a mass resolving power > 1200, a dynamic range of 10^6 and abundance sensitivity of 10^{-5}. This instrument was shown to be of particular use for extremely short transient signals (tens of µs up to ms range) generated by nanoparticles and microdroplets. Coupling this new TOFMS with laser ablation systems providing low signal dispersion[40] can lead to increased signal to noise ratios. Other types of simultaneous and quasi-simultaneous mass analysers exist, such as the Mattauch-Herzog sector-field mass spectrometer (MHMS)[41,42] or the ICPTOFMS Optimass[43], respectively. However, no data are currently available from these instruments for the analysis of minor and trace elements in small quantity of liquids.

The aim of the present study is to describe and determine the capabilities of SFMS and TOFMS for the analysis of fluid inclusions and to compare them to QMS, which is the state-of-the-art and the most frequently used instrument for the measurements of fluid inclusions by LA-ICPMS. In this objective, two types of samples have been analysed and the three instruments were evaluated and compared in terms of signal duration, intensity, precision, accuracy (when possible) and limits of detection (LODs). The first set of objects was consisting of sealed 20 µm inner diameter silica capillaries, containing multi-element (33 to 37) solutions with different set of concentrations (0.1, 1, 10 and 50 µg g^{-1}) and with Na fixed at a concentration of ca. 1000 µg g^{-1}. These capillaries mimic the configurations of small volumes of liquid trapped in a solid matrix, such as natural fluid inclusions, and have already been applied successfully to standardize the fluid inclusion analysis by LA-ICPMS.[44,45] They allow determining the achievable accuracy of the measurements for different concentrations of trace elements, as they are filled with solutions of known elemental concentrations. They moreover exhibit a much higher reproducibility compared to natural fluid inclusions, due to their fixed geometry and to their constant behaviour during laser ablation. A second set of objects are natural fluid inclusions selected from two origins and trapped within quartz crystals: (i) the first sample (BP-66-210, Alps) contains numerous two-phase (liquid + vapour) and low salinity fluid inclusions, with a homogeneous composition and variable diameters (from 5 to 100 µm), allowing to test precision and LODs of the three LA-ICPMS configurations for a wide range of fluid volumes; (ii) the second sample (7703-25, Zambia) contains multi-phase (liquid + vapour + solids) and high salinity fluid inclusions, but with a

smaller range of diameters (10 to 30 μm). The presence of several phases, including precipitates, makes the interpretation of the signals obtained for these inclusions with sequential ICPMS more challenging. In this respect, the capabilities of the TOFMS have been tested compared with QMS for the distinction between elements contained in fluid and solids and consequently for a better multi-elemental quantification of complex fluid inclusions.

2. Experimental

2.1. Instrumentation, operating conditions and data processing

All analyses were carried out at the Laboratory of Inorganic Chemistry at ETH Zürich (Switzerland). Three different configurations of LA-ICPMS were used for this study: a quadrupole (QMS) (Elan DRC Plus, PerkinElmer Inc., Ontario, Canada), a sector-field (SFMS) (Element 2, ThermoScientific, Bremen, Germany) and a prototype of time-of-flight (TOFMS) (Tofwerk AG, Thun, Switzerland). This prototype had been developed, by coupling an orthogonal TOF mass analyser (Tofwerk AG, Thun, Switzerland) with the ICP and vacuum interface of a commercial quadrupole-based ICPMS (Elan 6000, PerkinElmer/Sciex, Ontario, Canada) (see Borovinskaya *et al.*[14] for details). The same laser ablation system, namely a 193 nm GeoLas ArF Excimer (MicroLas, Göttingen, Germany), was coupled to the three ICPMS systems. A standard cylindrical ablation cell with relatively large internal volume was used for both QMS and SFMS configurations, as traditionally used for the analysis of fluid inclusions by sequential instruments.[4,6,28,31] For the TOFMS, a low dispersion tube cell, developed by Wang *et al.*[40], was used, which provides a higher signal to noise ratio per single laser pulse and can reduce the signal duration to less than 30 ms. Its use with a sequential mass spectrometer instrument, like QMS and SFMS, is problematic because signal aliasing will strongly deteriorate the attainable precision.[32] However, it is particularly beneficial in the case of TOFMS, by strongly increasing the signal/noise ratio, as shown in recent studies.[40,46] The cycle time in this paper is resembling the time necessary to produce a single data point in the transient signal. For sequential instruments, such as QMS and SFMS, the cycle time is given by the number of measured isotopes and by the time necessary for the analysis of each isotope (dwell time), plus the time necessary for the change of scanning mass windows (settling time). The Element 2 was configured to achieve lowest possible magnet settling times, reducing the cycle time by about a factor of two compared to the manufacturer

technical recommendations. For the configuration of TOFMS used, the quasi-simultaneous acquisition of all isotope signals is performed in 30 µs (cycle time). In our experiments, 1000 of these extractions were integrated before every data point was read out to reduce the total amount of data generated.[14] For simplicity, the cycle time for TOFMS in the text will be considered as 30 ms. The reader should, however, keep in mind that every cycle is an average of 1000 TOF extractions. The standard reference material NIST SRM 610 (reference values from Jochum *et al.*[47]) was used as external standard for the calibration of all analyses, and was analysed twice at the beginning and at the end for each set of samples to establish elemental sensitivity and to correct for instrumental drift.[29]

Operating conditions are given in Table 1, and are different between the measurement of multi-element solution in silica capillaries and the two types of natural fluid inclusions analysed (see 2.2 for sample description). Laser ablation of silica capillaries (see 3.1.) was realised with a frequency of 10 Hz, a laser spot diameter fixed at 32 µm and a theoretical fluence of 124 J cm^{-2} per pulse. Laser ablation of fluid inclusions (see 3.2. and 3.3.) was realised with a frequency of 10 Hz and using a stepwise opening procedure, as described in Günther *et al.*[3], starting the ablation with a laser spot diameter of 2 µm and stepwise increasing the spot diameter to the size of the fluid inclusion (from 5 to 90 µm), with a theoretical fluence between 16 and 500 J cm^{-2} per pulse. This procedure allows a controlled ablation by reducing the mechanical stress on the quartz surface, which limits the risk of splashing of the fluid.[3] LA-ICPMS were optimized for highest sensitivity for an intermediate m/Q range, while maintaining a ThO/Th < 0.5%, U/Th ~ 1 and Ba^{2+}/Ba^{+} < 3%, as determined on NIST SRM 610. Instrumental background signals (only from the gas blank) were measured for 20 s before each ablation for background correction and calculation of the limits of detection.[29] Helium was used as the carrier gas to transport the ablated material from the ablation cell to the ICPMS and argon was added via a laminar flow adapter before the ICP torch.[48] For the fast washout cell, a combination of argon and helium is used directly in the cell and so no additional make-up gas was used.[40] To increase the apparent magnet settling time on the Element 2, without increasing the actual magnet settling time, ^{22}Ne was introduced as a support mass. The earlier magnet settling together with the measurement time spent on ^{22}Ne helped to stabilise the magnet and improved the precision of the ^{23}Na intensity (measured using a E-Scan). For consistency, the support mass ^{22}Ne was also measured on the QMS. Due to a very high background, originating from previous experiments, the quantification of ^{11}B was compromised with the SFMS. Operating conditions for the TOFMS were chosen to maximize the transmission of high m/Q trace element isotopes thus

compromising the transmission of ions below m/Q = 9 within the notch filter upstream the TOFMS. Therefore, the sensitivity of these ions (including ^{7}Li) was insufficient for their detection at the concentrations used. Signal integration and absolute quantification were performed using the software StalQuant, developed at ETH Zürich (see details in Fricker49). The LODs were calculated according to the equation of Longerich *et al.*[29], since it is the most frequently method used in publications dealing with natural and synthetic fluid inclusions. For all analyses of silica capillaries and fluid inclusions, ^{23}Na was used as the internal standard for the quantification. For fluid inclusions, the Na content was estimated from the wt.% equivalent NaCl as determined by microthermometry.[50] Signal integration for capillaries and fluid inclusions was set on the basis of the Na total signal duration.

2.2. Materials

Three in-house multi-element solutions containing 33 elements (Li, B, Na, Mg, Al, K, Ca, Cr, Mn, Fe, Co, Ni, Cu, Zn, Ga, Ge, Sr, Nb, Ag, Cd, In, Sn, Ba, La, Tb, Hf, Ta, W, Pt, Tl, Pb, Bi, U) at concentrations of ca. 0.1, 1 and 10 µg g^{-1} each (except Na fixed at ca. 1000 µg g^{-1}) were prepared in 1% HNO_3 from single- and multi-element standard solutions (Inorganic Ventures, Merck). An in-house multi-element solution containing 37 elements (the 33 elements cited above + Rb, Cs, Ba and Sb) at a concentration of ca. 50 µg g^{-1} (except Na which was fixed at ca. 1000 µg g^{-1}) was also prepared. Silica capillaries (Photon Lines SAS, St-Germain-en-Laye, France) with an internal and external diameter of 20 µm and 150 µm respectively, and of ca. 1 cm length were filled with the solutions by capillarity and the ends were tipped with paraffin wax for sealing. An internal diameter of 20 µm was selected to mimic the typical size of natural fluid inclusions analysed by LA-ICPMS. Two types of natural fluid inclusions were selected from two different quartz samples for this study: (i) Two-phase (liquid + vapour) fluid inclusions from a quartz crystal from the French Alps (sample BP-66-210, Mont Blanc Massif, Pointe des Améthystes, see Fabre[51] for description). This sample contains numerous fluid inclusions, which are considered to be homogeneous in composition, as already shown by previous studies[45,51-53] of fluid inclusions in similar quartz crystals from the Mont Blanc Massif. These fluid inclusions have irregular shape and range from a few microns to 100 µm in diameter (Fig. 1a) and consequently from a few hundred pl to tens of nl in volume. At room temperature they are characterized by a dominant liquid aqueous phase with dissolved salts and a vapour phase of H_2O-CO_2-N_2 as determined by Raman spectroscopy, and no daughter minerals.[51] All fluid inclusions have a relatively homogeneous salinity of 4.8 ± 0.5

wt% NaCl equivalent as determined by microthermometry prior to LA-ICPMS analysis. The characteristics of its fluid inclusions (homogeneity in chemical composition and variability in size) make this sample a perfect experimental case study for the analytical comparison of the three LA-ICPMS setups; (ii) Multi-phase (liquid + vapour + multiple solids) fluid inclusions were selected from a quartz crystal from the western Zambian Copperbelt (sample 7703-25, Kabompo domes, Lolwa occurrence, see Eglinger *et al.*[54,55] for description). These fluid inclusions show irregular shape and range from 10 to 30 μm in diameter (Fig. 1b). They contain a dominant aqueous phase with dissolved salts, a vapour phase of H_2O-N_2-H_2 determined by Raman spectroscopy and numerous solids previously identified by Raman spectroscopy as calcium chloride hydrates, halite (NaCl), hematite (Fe_2O_3) and calcite ($CaCO_3$), plus other unidentified solids (Fig. 1b). All fluid inclusions have a high, relatively homogeneous salinity of 53-59 wt% $CaCl_2$ and 13-15 wt% NaCl equivalent as determined by microthermometry and their detailed composition, as determined by LA-ICPQMS, is given by Eglinger *et al.*[54] This sample was used in order to test the capabilities of the TOFMS for analysing complex, multi-phase and high-salinity fluid inclusions compared with the QMS. No analyses were performed with SFMS on this sample.

3. Results and discussion

3.1. Silica capillaries

3.1.1. Signals

Typical transient LA-ICPMS signals obtained from silica capillaries containing multi-element solutions of ca. 10 μg g^{-1} concentration are shown in Fig. 2. The oscillations observed in the transient signals from the TOFMS acquisition (Fig. 2c) corresponds to the 10 Hz frequency of the laser and demonstrates the low aerosol dispersion of the transport system employed with the short cycle time used (30 ms). The signal durations for the capillaries (determined based on the ^{23}Na signal) are typically longer than 20 s for the high dispersion transport system used for QMS and SFMS, while this is reduced to about 4 s for the tube cell used for TOFMS. With a cycle time of 468 ms for QMS, 887 ms for SFMS and 30 ms for TOFMS, the signal durations correspond to ca. 47, 27 and 133 data points respectively. Peak signal/background ratios for ^{23}Na are similar for the three setups, with ca. 5×10^3 for QMS, 6×10^2 for SFMS

and 10^3 for TOFMS. For the four tested solutions, the lighter isotopes (^{7}Li and ^{11}B) are barely detected by TOFMS due to the optimization setting used for these experiments (see 2.1.). At high concentrations (ca. 50 µg g^{-1}), all elements added to the solutions are detected by QMS, SFMS and TOFMS, except for ^{11}B by SFMS and ^{7}Li by TOFMS (due to elevated backgrounds). At low concentrations (ca. 0.1 µg g^{-1}), only isotopes with m/Q > 88 are detected on average by QMS and SFMS, whereas TOFMS detects only isotopes with m/Q > 139.

3.1.2. Precision and accuracy

The precision and accuracy were calculated from means and standard deviations for a series of measurements of different silica capillaries (n = 4 to 7) for each solution (0.1, 1, 10, 50 µg g^{-1}) and for all the isotopes listed in Table 2. The precision is represented by the relative standard deviation (RSD) expressed in % for a series of measurements and is defined by equation (1).

(1) $$RSD_i = \frac{s_i}{m_i} \times 100\%$$

where s_i and m_i are respectively the standard deviation (1σ) and the mean of the measurements (n = 4 to 7) for one isotope i.

The accuracy is represented by the relative error (RE) expressed in % between the expected concentration of one isotope i in each selected solution (C_i) and the mean concentration calculated from the LA-ICPMS analyses (C_m) of the same solution trapped in different silica capillaries (n = 4 to 7) as defined by equation (2).

(2) $$RE_i = \frac{(C_m - C_i)}{C_i} \times 100\%$$

The value of accuracy is therefore negative if the calculated mean concentration from LA-ICPMS analyses is underestimated and positive if it is overestimated. The precision and accuracy values obtained for the four solutions and for five isotopes (^{7}Li, ^{65}Cu, ^{88}Sr, ^{139}La, ^{209}Bi), selected from the low to high atomic masses, are presented in Fig. 3 and Fig. 4 respectively. The full dataset for solutions with 33 elements (at ca. 0.1, 1 and 10 µg g^{-1}) or 37 elements (at ca. 50 µg g^{-1}) is given in Table 2. RSD values are typically within 9 to 30% for

QMS and 6 to 60% for SFMS, using the same cylindrical ablation cell, and within 3 to 40% for TOFMS (except ^{7}Li) using the fast washout cell, depending on concentrations and detected isotopes (Fig. 3, Table 2). The RSD values of the measured isotopes are not depending on the concentration of the different solutions for the three investigated setups and are not directly correlated with the signal intensity. These findings indicate that the analytical precision is likely dominated by the laser ablation behaviour (non-continuous ablation of liquid) and not by counting statistics. RE values are typically within -40 to 40% for QMS, -50 to 50% for SFMS and -30 to 30% for TOFMS, for all concentrations and isotopes when detected (Fig. 4, Table 2), and generally tend to be higher at low concentration. Anomalously high RSD and RE values are occasionally found for some isotopes such as ^{57}Fe (RSD up to 125%, RE up to 170%), ^{118}Sn (RSD up to 122%, RE up to 47%) or ^{205}Tl (RSD up to 67%, RE down to -74%). For isotopes such as ^{57}Fe, this can be related to polyatomic interferences of $^{40}Ar^{16}O^{1}H$. For other isotopes such as ^{118}Sn, ^{181}Ta or ^{205}Tl, these variabilities could be either due to a problem of stability of these elements in solution or to a problem during solution preparation. The fact that Ba in the 50 µg g^{-1} solution is consistently found at twice the reference values is most likely explained by an error in sample preparation. Consequently, these five elements are not considered in the final evaluation.

3.1.3. Limits of detection

LODs calculated from means of the individual acquisitions (n = 5 to 6) for the QMS, SFMS and TOFMS are presented in Fig. 5 for the solutions at concentration of ca. 10 µg g^{-1} and the dataset for all the tested solutions is given in Table 2. The LODs do not depend of the concentration of the different solutions for a same instrument. The observed differences reflect only the variations in fillings of the capillary or the quantity of fluid removed during laser ablation. For the three instruments, LODs decrease of ca. two to three orders of magnitude from low to high atomic mass. The highest LODs are typically within 5 to 30 µg g^{-1} for light isotopes ($m/Q < 57$) for the QMS and SFMS (except for ^{11}B) and within 10 to 20 µg g^{-1} for the TOFMS (except for ^{7}Li). The lowest LODs are typically within 0.01 and 0.1 µg g^{-1} for heavy isotopes ($m/Q > 139$) for the SFMS and TOFMS and between 0.1 to 1 µg g^{-1} for the QMS. For intermediate isotopes with $57 \leq m/Q \leq 139$, SFMS shows systematically lower LODs than the QMS and SFMS within up to one order of magnitude of ca. 0.05 µg g^{-1} for $m/Q < 88$. QMS and TOFMS have similar LODs within the same order of magnitude of ca. 0.5-3 µg g^{-1} and 0.01-0.5 µg g^{-1} for light and heavy isotopes respectively, but TOFMS tends to

have slightly lower LODs than QMS for isotopes with m/Q > 111 (Fig. 5, Table 2). Compared to the QMS, LODs are lower for SFMS and TOFMS, and are in the same order of magnitude of ca. 0.01 μg g^{-1} for m/Q > 159 for both SFMS and TOFMS.

3.2. Two-phase fluid inclusions

3.2.1. Signals

Typical transient LA-ICPMS signals for 25 μm two-phase fluid inclusions from sample BP-66-210 (Mont Blanc Massif, French Alps) are shown in Fig. 6. The signal durations after opening the fluid inclusions mainly depend on the inclusion size (Fig. 7), the salinity being identical for all fluid inclusions. For inclusions of 25 μm in size, the cylindrical ablation cell led to signal durations typically of ca. 26 s with the QMS and 22 s with the SFMS, while the fast washout tube cell reduced the signal length to ca. 9 s. With a cycle time of 273 ms for QMS, 560 ms for SFMS and 30 ms for TOFMS (Table 1), the signal durations correspond to ca. 95, 39 and 300 data points respectively. Within the two-phase fluid inclusions, 9 isotopes (^{7}Li, ^{11}B, ^{23}Na, ^{25}Mg, ^{35}Cl, ^{85}Rb, ^{88}Sr, ^{133}Cs and ^{137}Ba) could be detected with the QMS, 10 isotopes (^{7}Li, ^{23}Na, ^{35}Cl, ^{44}Ca, ^{85}Rb, ^{88}Sr, ^{133}Cs, ^{137}Ba, ^{182}W and ^{208}Pb) with the SFMS, whereas 14 isotopes (^{11}B, ^{23}Na, ^{25}Mg, ^{35}Cl, ^{39}K, ^{55}Mn, ^{75}As, ^{85}Rb, ^{88}Sr, ^{121}Sb, ^{133}Cs, ^{137}Ba, ^{182}W and ^{208}Pb) were detected using the TOFMS. Considering the ratios normalized to ^{23}Na, only the first seconds of the fluid inclusions signals show constant values (5 s for QMS, 9 s for SFMS and 1.5 s for TOFMS). This corresponds to ca. 96 to 98% of the integrated ^{23}Na intensity of the fluid inclusions signals and ca. 18, 16 and 52 data points for QMS, SFMS and TOFMS respectively (Fig. 6). Peak signal/background ratios for ^{23}Na are ca. 10^4 for QMS, 2 × 10^3 for SFMS and 9 × 10^3 for TOFMS respectively. Peak signal/background ratios for minor and trace elements are in the same order of magnitudes for the three configurations (Fig. 6).

3.2.2. Concentration, standard deviation and precision

The concentrations for the two-phase fluid inclusions analysed (sample BP-66-210, Alps) are presented for the three instruments (QMS, SFMS and TOFMS) and as function of their diameter (in ranges of < 10 μm, 10-25 μm and > 25 μm) in Fig. 8. The calculated mean concentrations, standard deviations (1σ) and precisions (RSD) for all fluid inclusions are

given in Table 3. The isotopes ^{35}Cl, ^{85}Rb, ^{88}Sr and ^{133}Cs, ^{137}Ba were systematically detected by the three LA-ICPMS configurations and for fluid inclusions > 10 µm, with a good reproducibility of the measurements. The mean concentrations and standard deviations for the QMS, SFMS and TOFMS are respectively of 4110 ± 7640, 1100 ± 710 and 19000 ± 5140 µg g^{-1} for ^{35}Cl, 210 ± 80, 155 ± 127 and 113 ± 37 µg g^{-1} for ^{85}Rb, 55 ± 30, 49 ± 36 and 36 ± 10 µg g^{-1} for ^{88}Sr, 70 ± 35, 62 ± 65 and 35 ± 13 µg g^{-1} for ^{133}Cs and 10 ± 20, 6.5 ± 8 and 7.4 ± 5 µg g^{-1} for ^{137}Ba (Table 3). The RSD calculated for all fluid inclusions vary considerably and range within 33 to 200% for QMS (n=35), 10 to 182% for SFMS (n=24) and 23 to 167% for TOFMS (n=40) respectively. For the detected elements, RSDs calculated appear lower for the TOFMS compared to QMS and SFMS respectively, suggesting an improvement in terms of precision achieved by the quasi-simultaneous detection. In all cases, however, the calculated RSDs for fluid inclusions are higher compared to silica capillaries due to their variability in size, shape and depth. Other isotopes are detected sporadically by the three instruments, such as ^{25}Mg, ^{137}Ba or ^{182}W, and are characterized by higher standard deviations (Table 3). ^{79}Br was detected in the fluid inclusions by the three instruments, but was not quantified because of the uncertain reference value for NIST SRM 610 used for calibration.[47] Additional isotopes, detected by the TOFMS in fluid inclusions > 10 µm, are ^{39}K, ^{55}Mn, ^{75}As and ^{121}Sb, which were not included in the isotope selection for the QMS and SFMS. On the other hand, the isotopes ^{59}Co, ^{65}Cu or ^{66}Zn were not detected by the three instruments due to concentrations below LODs (Table 3).

Small fluid inclusions (< 10 µm) were also measured with the three instruments, but relatively few data were obtained for this sample set. Nevertheless, results obtained show that TOFMS still detects five isotopes (^{35}Cl, ^{85}Rb, ^{88}Sr, ^{133}Cs and ^{208}Pb) in addition to ^{23}Na, whereas QMS and SFMS detect only one to two isotopes (^{85}Rb and/or ^{133}Cs). As shown in Fig. 9, the analysis of a 5 µm fluid inclusion by QMS allows only the detection of the ^{23}Na signal, present as the major isotope. Minor isotopes such as ^{85}Rb, ^{88}Sr and ^{133}Cs cannot be detected by QMS, but were detected using the TOFMS. Detection of ^{35}Cl signal is improved with the TOFMS, which represents a major benefit for the quantification of fluid inclusions based on their chlorinity.[25] Considering signal to background ratios of different isotopes as function of ^{23}Na signal to background ratio for a 25 µm fluid inclusion analysed by TOFMS (Fig. 10), it appears that all isotopes show a linear positive correlation with the ^{23}Na used as internal standard. The correlation is particularly strong for the first 1.3 s of the signal, which represents 95% of the total ^{23}Na intensity and corresponds to ca. 44 measurements cycles. About 90% of fluid inclusions total ^{23}Na intensity is contained in the first 0.7 s, which

corresponds to ca. 24 measurements cycles (Fig. 10). Due to its quasi-simultaneous detection, quantification of two-phase fluid inclusions with the TOFMS could be consequently realised on one data point at the maximum peak intensity of the ^{23}Na signal, corresponding to the first 30 ms of the signal.

3.2.3. Limits of detection

LODs calculated for fluid inclusions from means of individual acquisitions (n=24 to 40) for the QMS, SFMS and TOFMS are given in Table 3. As shown in Fig. 11, the LODs are inversely correlated to the inclusion diameter with a parabolic decrease, regardless of the element considered. LODs calculated for isotopes analysed by QMS, SFMS and TOFMS and variable diameters of fluid inclusions (< 10 µm, 10-25 µm and > 25 µm) are shown in Fig. 12. For fluid inclusions > 25 µm, LODs for QMS and TOFMS are within the same order of magnitude, varying typically within 10^1 to 10^4 µg g^{-1} for light isotopes ($m/Q \leq 57$) and within 10^{-1} to 10^1 µg g^{-1} for heavy isotopes ($m/Q \geq 85$), whereas SFMS shows the lowest LODs, generally within one to two orders of magnitude below QMS and TOFMS. For fluid inclusions between 10 and 25 µm in diameter, LODs for SFMS and TOFMS are within the same order of magnitude, varying between 10^2 to 10^5 µg g^{-1} for light isotopes ($m/Q \leq 57$) and between 1 to 10^3 µg g^{-1} for heavier isotopes. LODs for QMS tend to be higher by ca. one order of magnitude compared to TOFMS and SFMS. For fluid inclusions < 10 µm, the lowest LODs are achieved by TOFMS, varying within 10^2 to 10^5 µg g^{-1} for $m/Q < 85$ and within 10^1 to 10^2 µg g^{-1} for $m/Q > 85$, for which they are lower by ca. one order of magnitude compared to those of QMS and SFMS. Thus, the size of fluid inclusions strongly constrains the achievable LODs of each instrument and the results show particularly that TOFMS provide the lowest LODs for fluid inclusions with diameter ≤ 10 µm.

3.3. Multi-phase fluid inclusions

3.3.1. Signal structure

Typical transient signals from QMS and TOFMS acquisition of 15 µm multi-phase (liquid + vapour + solids) fluid inclusions from sample 7703-25 (Kabompo domes, Zambia) are shown in Fig. 13. The signal durations (based on ^{23}Na) obtained for such fluid inclusions are longer

than those obtained for fluid inclusions of similar size from the Alps (sample BP-66-210) due to their higher salinities and last for ca. 60 s for QMS and ca. 20 s for TOFMS. With a cycle time of 195 ms for QMS and 30 ms for TOFMS (Table 1), this corresponds to ca. 307 and 667 acquisitions cycles respectively. Peak signal/background ratios for ^{23}Na are ca. 10^3 for QMS and 2×10^2 for TOFMS. The QMS allows the detection of 13 isotopes (^{23}Na, ^{25}Mg, ^{39}K, ^{44}Ca, ^{47}Ti, ^{57}Fe, ^{65}Cu, ^{85}Rb, ^{88}Sr, ^{95}Mo, ^{137}Ba, ^{208}Pb and ^{238}U) on the 15 measured, whereas TOFMS detects 38 isotopes (^{23}Na, ^{24}Mg, ^{25}Mg, ^{26}Mg, ^{27}Al, ^{35}Cl, ^{39}K, ^{55}Mn, ^{57}Fe, ^{59}Co, ^{64}Zn, ^{65}Cu, ^{66}Zn, ^{67}Zn, ^{68}Zn, ^{85}Rb, ^{86}Sr, ^{88}Sr, ^{95}Mo, ^{96}Mo, ^{97}Mo, ^{98}Mo, ^{130}Te, ^{133}Cs, ^{135}Ba, ^{136}Ba, ^{137}Ba, ^{138}Ba, ^{139}La, ^{140}Ce, ^{141}Pr, ^{143}Nd, ^{205}Tl, ^{206}Pb, ^{207}Pb, ^{208}Pb, ^{209}Bi and ^{238}U) on the whole analysed mass range.

The signals obtained for QMS for all detected isotopes have all the same shape and are correlated in time, as observed in Fig. 13 by constant ratios normalized to ^{23}Na. The different solids (halite, calcite, hydrates, hematite) observed in the fluid inclusions by optical microscopy and determined by Raman spectroscopy are consequently not individualized with QMS.[54] For a similar 15 µm multi-phase fluid inclusion, the liquid and solid phases are properly discriminated during TOFMS measurement, with the signals of the majority of the detected isotopes displaying specific shapes during acquisition. This confirms that elements or groups of elements are present in different physical phases within the fluid inclusions, as previously observed by microscopy and Raman spectroscopy. The observed elemental discrimination, shown here for the first time using TOFMS, is possible only due to the fast washout of the ablation cell used in combination with the quasi-simultaneous detection of the TOF mass analyser. The different phases present within the fluid inclusion are thus not dispersed significantly within the ablation cell and are transported separately during laser ablation to the MS. As a result, the signals of Rb-Sr-Cu-Al-Pb-Ba-Cs, Na-Mg-K-Cl and Fe-Mn-Ti could be interpreted respectively as those of the aqueous phase, hydroxides and hematite crystals, as previously identified by Raman spectroscopy.[54] However, some signals are mixed and could indicate a partitioning of the elements between different phases. The ^{23}Na signal is not completely correlated to the signal of ^{35}Cl, which is probably due to quasi-simultaneous ablation of NaCl solid and liquid phase in which Na and Cl are major solutes but present in different proportions to NaCl. The same observation is made with the Ba isotopes, which show a common signal shape compared to those of Rb and Sr isotopes, but with minor differences, suggesting that Ba could be present both in the aqueous phase and in a solid phase (*e.g.* barite, $BaSO_4$) not identified previously by Raman spectroscopy. The signal of ^{65}Cu is partially correlated with those of ^{64}Zn, ^{66}Zn, ^{67}Zn and ^{68}Zn, suggesting that

these elements are likely associated within a single phase. Finally, the signal of U shows a peak clearly distinct from the other signals, and correlated with the one of Mo (not shown), indicating that these two elements are present in an independent phase and not as a solute in the aqueous phase. However, the presence of a U-bearing mineral is not common in these fluid inclusions, since its signal has not been detected systematically here.

Discrimination between elements in fluid phase and daughter minerals has been previously observed by LA-ICPMS (Günther *et al*.[3] for the first occurrence), but this was obtained for large-size (> 40 μm in diameter) and high-salinity fluid inclusions[3,4,38], and could not be reached for the tested small fluid inclusions, as demonstrated by the QMS results (Fig. 13). These previous observations suggest that the aerosol dispersion in the large volume ablation cells does not allow distinguishing the different phases at such extent. This preliminary result requires an extensive investigation, in particular, by testing the capabilities and the limits on synthetic fluid inclusions in comparison with natural multi-phase fluid inclusions from different geological contexts. Nevertheless, this result opens interesting perspectives, for instance to allow: (i) identification of solids difficult to analyse by Raman spectroscopy (small size and/or transparent solids) and (ii) detailed analysis of minor to trace elements concentrations within solids.

3.3.2. Concentrations, standard deviations, precisions and limits of detection

The calculated mean concentrations, standard deviations (1σ) and precisions (RSD) for multi-phase fluid inclusions from sample 7703-25 for QMS and TOFMS are presented in Table 4. The major input of TOFMS is the detection of 38 isotopes on the whole mass range, with particularly the discrimination of several isotopes of a same element, such as Mg, Zn, Mo, Ba and Pb isotopes (Table 4), with a good reproducibility. Concentrations are variable among the analysed fluid inclusions, in particular for isotopes such as ^{39}K, ^{65}Cu or ^{57}Fe for instance, resulting in relatively high RSD. For isotopes detected both by QMS and TOFMS, the calculated RSD are lower on average for TOFMS, as already shown for two-phase fluid inclusions, and range within 39 to 154% and 6 to 100% for QMS and TOFMS, respectively. Considering that these fluid inclusions have approximately the same dimension (10 to 25 μm), these variations are likely related to a heterogeneous trapping of the fluid during the quartz crystallization. The calculated LODs for QMS and TOFMS show the same results as for the two-phase fluid inclusions, that is similar LODs for QMS and TOFMS for $m/Q < 57$ and lower LODs for TOFMS for heavy isotopes ($m/Q > 95$).

4. Summary and conclusions

Three different configurations of LA-ICPMS, namely a quadrupole (QMS), a sector-field (SFMS) and an orthogonal time-of-flight (TOFMS), were tested in this study in order to address their respective capabilities for sequential (QMS, SFMS) and quasi-simultaneous (TOFMS) multi-element analysis of small quantities of liquids (pl to nl) contained in silica capillaries and in natural fluid inclusions.

The two sets of objects studied, namely multi-element solutions in silica capillaries and natural fluid inclusions, allowed to evaluate the capabilities of SFMS and TOFMS and to compare them to QMS, which is currently the traditionally used and state-of-the-art instrument for the measurements of fluid inclusions by LA-ICPMS. The main results obtained in this study are: (i) QMS, SFMS and TOFMS have similar signal to background ratios for ^{23}Na within the same order of magnitude of ca. 10^3 to 10^4, those of QMS being slightly higher to the other ones; (ii) Signals durations are similar (20-30 s) for silica capillaries and two-phase fluid inclusions using a standard cylindrical ablation cell with QMS and SFMS, but are 2 to 30 times shorter (1-15 s) using the fast washout tube cell in combination with the TOFMS. In the case of high-salinity and multi-phase fluid inclusions, the signals durations are longer and last for ca. 60 s and 20 s for QMS and TOFMS, respectively; (iii) Cycle times for covering the range of measured masses with QMS and SFMS are ca. 10 to 30 longer compared to those of TOFMS, where cycle time is only 30 ms for quasi-simultaneous measurement of the entire mass range, resulting in a number of cycles of ca. 2 to 5 times higher compared to QMS and SFMS and compensating for the multiplicative noise in the ICPMS; (iv) RSD calculated are on average lower for TOFMS compared to QMS and SFMS, for all measured isotopes, indicating better precision achievable by TOFMS; (v) LODs for silica capillaries are approximately 10 times lower for SFMS compared to QMS and TOFMS for isotopes with $m/Q < 137$ (except ^{11}B) and almost equivalent for SFMS and TOFMS for heavier isotopes and ca. 3 times lower than for QMS. For fluid inclusions, LODs are inversely correlated to the inclusion diameter with a parabolic decrease. SFMS presents lower LODs of ca. one order of magnitude compared to QMS and TOFMS for diameter > 25 µm, whereas TOFMS achieve the lower LODs for inclusions < 10 µm, with one order of magnitude below SFMS and QMS for isotopes with $m/Q > 85$.

Consequently, the present study demonstrates that SFMS and TOFMS provide improvements, particularly in terms of precision and LODs, compared to the QMS instrumentation tested, and leads to the following conclusions:

(1) QMS is a very efficient instrument for the multi-element analysis of fluid inclusions, with good reproducibility, precisions and accuracies, but is limited by relatively high LODs compared to SFMS and TOFMS, in particular for heavy isotopes, and by a limited set of measureable elements (generally less than 20) due to a compromise between signal duration and cycle time.

(2) SFMS has the great advantage to reduce LODs within one order of magnitude compared to QMS and TOFMS, especially for light isotopes, but has longer acquisition times, due to the necessary magnet jumps, which limits the number of measureable elements and the attainable precision. It is consequently a well-adapted instrument for the precise measurement of a few isotopes (< 5) present at low concentrations in fluid inclusions.

(3) TOFMS presents both advantages to have rapid, quasi-simultaneous data acquisition for all isotopes from ^{6}Li to ^{238}U in a cycle time of 30 µs. The precisions were found to be better than for QMS and SFMS and LODs are slightly higher or even similar than SFMS for heavy isotopes and lower for small fluid inclusions. Using TOFMS coupled to the fast washout ablation cell, which improves considerably the signal to noise ratio by decreasing the aerosol dispersion, allows detection of small-size (< 10 µm) and low-salinity fluid inclusions. Its application to complex multi-phase and high-salinity fluid inclusions allows discrimination of signals of the different phases (liquid and solids), as well as the detection of a higher number of isotopes, even for a same element. Moreover, detection of ^{35}Cl is improved with the TOFMS, which could represent a major benefit for the quantification of fluid inclusions based on their chlorinity.

In conclusion, the orthogonal TOFMS reveals to be a highly promising instrument for the multi-element analysis of fluid inclusions, particularly since it provides fast and relatively complete information on fluid inclusions composition. Its use is consequently of high interest for the study of geological fluids, which are characterized by an extremely wide variety of chemical elements, potentially from Li to U, with a very variable range of concentrations, from a few parts per billions (ppb) to tens of percents. Future applications could be considered in particular for the analysis of melt inclusions by TOFMS (*e.g.* Pettke *et al.*[57]), but also for the measurement of isotopic ratios in fluid inclusions (*e.g.* Pettke *et al.*[33]). By

extension, these results demonstrate the analytical potential of the TOFMS for the determination of minor and trace elements in small volumes of liquids (pl to nl) trapped in various solid matrices.

Acknowledgements

This work was supported by the CNRS through the national call CESSUR (INSU) with a financial grant given to Dr. Julien Mercadier in 2014 and by the Labex Ressources 21 through the national program "Investissements d'avenir" with the reference ANR-10-LABEX-21-RESSOURCES21. The authors are highly thankful to Dr. Marie-Christine Boiron and Dr. Aurélien Eglinger for supplying the quartz samples. We would like also to thank Dr. Bodo Hattendorf for the helpful discussions and comments. Two anonymous reviewers are also thanked for their constructive comments that helped to improve the manuscript.

References

1. S. Gschwind, L. Flamigni, J. Koch, O. Borovinskaya, S. Groh, K. Niemax and D. Günther, *J. Anal. At. Spectrom.*, 2011, **26**, 1166-1174.
2. S. Gschwind, H. Hagendorfer, D. A. Frick and D. Günther, *Anal. Chem.*, 2013, **85**, 5875–5883.
3. D. Günther, A. Audétat, R. Frischknecht and C. A. Heinrich, *J. Anal. At. Spectrom.*, 1998, **13**, 263-270.
4. C. A. Heinrich, T. Pettke, W. E. Halter, M. Aigner-Torres, A. Audétat, D. Günther, B. Hattendorf, D. Bleiner, M. Guillong and I. Horn, *Geochim. Cosmochim. Acta*, 2003, **67**, 3473-3497.
5. M. M. Allan, B. W. D. Yardley, L. J. Forbes, K. I. Shmulovich, D. A. Banks and T. J. Shepherd, *Am. Miner.*, 2005, **90**, 1767-1775.
6. T. Pettke, F. Oberli, A. Audétat, M. Guillong, A. C. Simon, J. J. Hanley, L. M. Klemm, *Ore Geology Reviews*, 2012, **44**, 10-38.
7. K. Rauchenstein-Martinek, T. Wagner, M. Wälle and C. A. Heinrich, *Chem. Geol.*, 2014, **385**, 70-83.

8. M. Albrecht, I. T. Derrey, I. Horn, S. Schuth and S. Weyer, *J. Anal. At. Spectrom.*, 2014, **29**, 1034-1041.
9. D. J. Kutscher, M. B. Fricker, B. Hattendorf, J. Bettmer and D. Günther, *Anal. Bioanal. Chem.*, 2011, **401**, 2691-2698.
10. H-F. Hsieh, W-S. Chang, Y-K. Hsieh and C-F. Wang, *Anal. Chim. Acta*, 2011, **669**, 6-10.
11. U. Kumtabtim, A. Siripinyanond, C. Auray-Blais, A. Ntwari and J. S. Becker, *Int. J. Mass. Spectrom.*, 2011, **307**, 174-181.
12. M. Krachler, J. Zheng, D. Fisher and W. Shotyk, *Anal. Chim. Acta*, 2005, **530**, 291-298.
13. E. Ciceri, S. Recchia, C. Dossi, L. Yang and R. E. Sturgeon, *Talanta*, 2008, **74**, 642-647.
14. O. Borovinskaya, B. Hattendorf, M. Tanner, S. Gschwind and D. Günther, *J. Anal. At. Spectrom.*, 2013, **28**, 226-233.
15. E. Roedder, 1984. In: P. H. Ribbe (Ed.), Reviews in Mineralogy: Mineralogical Society of America, vol. 12, 646 pp.
16. R. H. Goldstein, *Lithos*, 2001, **55**, 159-193.
17. J. L. R. Touret, *Lithos*, 2001, **55**, 1-25.
18. M. Scambelluri and P. Philippot, *Lithos*, 2001, **55**, 213-227.
19. M. P. Smith, V. Savary, B. W. D. Yardley, J. W. Valley, J. J. Royer and M. Dubois, *J. Geophys. Res.*, 1998, **103**, 27223-27237.
20. S. F. Simmons, M. P. Simpson and T. J. Reynolds, *Econ. Geol.*, 2007, **102**, 127-135.
21. I.A. Munz, *Lithos*, 2001, **55**, 195-212.
22. R. C. Burruss. In: L. Samson, A. Andersen and D. Marshall (Eds.), 2003, **32**, 159-174.
23. A. Audétat, D. Günther and C. A. Heinrich, *Science*, 1998, **279**, 2091-2094.
24. T. Ulrich, D. Günther and C. A. Heinrich, *Nature*, 1999, **399**, 676-679.
25. J. J. Wilkinson, B. Stoffell, C. C. Wilkinson, T. E. Jeffries, and M. S. Appold, *Science*, 2009, **323**, 764-767.
26. A. Richard, C. Rozsypal, J. Mercadier, D. A. Banks, M. Cuney, M-C. Boiron and M. Cathelineau, *Nat. Geosci.*, 2012, **5**, 142-146.
27. T. J. Shepherd and S. R. Chenery, *Geochim. Cosmochim. Acta*, 1995, **59**, 3997-4007.
28. D. Günther, R. Frischknecht, C. A. Heinrich and H. J. Kahlert, *J. Anal. At. Spectrom.*, 1997, **12**, 939-944.
29. H. P. Longerich, S. E. Jackson and D. Günther, *J. Anal. At. Spectrom.*, 1996, **11**, 899-904.
30. T. U. Schlegel, M. Wälle, M. Steele-MacInnis and C.A. Heinrich, *Chem. Geol.*, 2012, **334**, 144-153.

31. M. Wälle and C. A. Heinrich, *J. Anal. At. Spectrom.*, 2014, **29**, 1052-1057.
32. T. Pettke, C. A. Heinrich, A. C. Ciocan and D. Günther, *J. Anal. At. Spectrom.*, 2000, **15**, 1149-1155.
33. T. Pettke, F. Oberli, A. Audétat, U. Wiechert and C. A. Heinrich, *J. Anal. At. Spectrom.*, 2011, **26**, 475-492.
34. T. Pettke, F. Oberli and C. A. Heinrich, *Earth Planet. Sci. Lett.*, 2010, **296**, 267-277.
35. D. P. Myers and G. M. Hieftje, *Microchem. J.*, 1993, **48**, 259-277.
36. M. Tanner and D. Günther, *Anal. Bioanal. Chem.*, 2008, **391**, 1211-1220.
37. M. Tanner and D. Günther, *Anal. Chim. Acta*, 2009, **633**, 19–28.
38. D. Bleiner, K. Hametner and D. Günther, *Fresen J. Anal. Chem.*, 2000, **368**, 37-44.
39. H. Chen, T. K. Kyser and A. H. Clark, *Miner. Deposita*, 2011, **46**, 677-706.
40. H. A. O. Wang, D. Grolimund, C. Giesen, C. N. Borca, J. R. H. Shaw-Stewart, B. Bodenmiller and D. Günther, *Anal. Chem.*, 2013, **85**, 10107–10116.
41. G. D. Schilling, F. J. Andrade, J. H. Barnes, R. P. Sperline, M. B. Denton, C. J. Barinaga, D. W. Koppenaal and G. M. Hieftje, *Anal. Chem.*, 2007, **79**, 7662-7668.
42. M. Resano, K. S. McIntosh and F. Vanhaecke, *J. Anal. At. Spectrom.*, 2012, **27**, 165-173.
43. R. E. Sturgeon, J. W. H. Lam and A. Saint, *J. Anal. At. Spectrom.*, 2000, **15**, 607-616.
44. B. Stoffell, M. S. Appold, J. J. Wilkinson, N. A. McClean and T. E. Jeffries, *Econ. Geol.*, 2008, **103**, 1411–1435.
45. M. Leisen, M-C. Boiron, A. Richard and J. Dubessy, *Chem. Geol.*, 2012, **330-331**, 197-206.
46. C. Giesen, H. A. O. Wang, D. Schapiro, N. Zivanovic, A. Jacobs, B. Hattendorf, P.J. Schüffler, D. Grolimund, J. M. Buhmann, S. Brandt, Z. Varga, P. J. Wild, D. Günther and B. Bodenmiller, *Nat. Methods*, 2014, **11**, 417-422.
47. K. P. Jochum, U. Weis, B. Stoll, D. Kuzmin, Q. Yang, I. Raczek, D. E. Jacob, A. Stracke, K. Birbaum, D. A. Frick, D. Günther and J. Enzweiler, *Geostandards and Geoanalytical Research*, 2011, **35**, 397–429.
48. S. M. Eggins, L. P. J. Kinsley and J. M. G. Shelley, *Appl. Surf. Sci.*, 1998, **127-129**, 278-286.
49. M. B. Fricker, 2012. Design of ablation cells for LA-ICP-MS: from modeling to high spatial resolution analysis applications, PhD thesis, ETH Zürich.
50. R. J. Bodnar, 2003. In: I. Samson, A. Anderson and D. Marshall (eds), Fluid inclusions: Analysis and Interpretation, *Mineral. Assoc. Canada*, **32**, 81-99.

51. C. Fabre, 2000. Reconstitution chimique des paléofluides par spectrométrie d'émission optique couplée à l'ablation laser. Applications aux fluides alpins et aux fluides de bassins. PhD thesis, Université Nancy.
52. C. Fabre, M-C. Boiron, J. Dubessy and A. Moissette, *J. Anal. At. Spectrom.*, 1999, **14**, 913-922.
53. C. Fabre, M-C. Boiron, J. Dubessy, M. Cathelineau and D. Banks, *Chem. Geol.*, 2002, **182**, 249-264.
54. A. Eglinger, C. Ferraina, A. Tarantola, A-S. André-Mayer, O. Vanderhaeghe, M-C. Boiron, J. Dubessy, A. Richard and M. Brouand, *Contrib. Mineral. Petrol.*, 2014, **167:967**, 1-28.
55. A. Eglinger, A. Tarantola, C. Durand, C. Ferraina, O. Vanderhaeghe, A-S. André-Mayer, J-L. Paquette and E. Deloule, *Chem. Geol.*, 2014, **386**, 218-237.
56. A. Audétat, T. Pettke, C.A. Heinrich and R.J. Bodnar, *Econ. Geol.*, 2008, **103** (5), 877-908.
57. T. Pettke, W. E. Halter, J. D. Webster, M. Aigner-Torres and C. A. Heinrich, *Lithos*, 2006, **78**, 333-361.

Tables captions

Table 1: Operating conditions and acquisition parameters used for this study.

Table 2: Nominal and measured compositions of silica capillaries with internal diameter of 20 µm containing multi-element solutions at concentration of ca. 0.1, 1, 10 and 50 µg g^{-1} analysed by LA-ICPQMS, LA-ICPSFMS and LA-ICPTOFMS. The analytical conditions are given in Table 1. SD: standard deviation; LOD: limit of detection; n.m.: not measured; n: number of analyses.

Table 3: Chemical compositions of two-phase fluid inclusions from sample BP-66-210 (Mont Blanc Massif, French Alps) analysed by LA-ICPQMS, LA-ICPSFMS and LA-ICPTOFMS. See Table 1 for the analytical conditions. The limits of detections (LOD) are reported as a function of the fluid inclusions diameter (< 10 µm, 10-25 µm and > 25 µm respectively). FI: fluid inclusion; n: number of fluid inclusions analysed; SD: standard deviation; RSD: relative standard deviation; n.m.: not measured.

Table 4: Chemical compositions of multi-phase fluid inclusions from sample 7703-25 (Kabompo domes, Zambia) analysed by LA-ICPQMS and LA-ICPTOFMS. See Table 1 for the analytical conditions. SD: standard deviation; LOD: limit of detection; n: number of analyses.

Figures captions

Fig. 1: Microphotographs in transmitted light of fluid inclusions observed at room temperature from selected quartz (Qtz) samples. (a) Two-phase fluid inclusions (sample BP-66-210, Mont Blanc Massif, Pointe des Amethystes, French Alps) containing a dominant aqueous phase with dissolved salts (L_{aq}) and a vapour phase (V). This sample contains numerous 5 to 100 µm fluid inclusions of this type with high compositional homogeneity. (b) Multi-phase fluid inclusion (sample 7703-25, Kabompo domes, Lolwa occurence, Zambia) containing a dominant aqueous phase with dissolved salts (L_{aq}), a vapour phase (V) and various solids: calcium chloride hydrates (Hyd), halite (Hl), hematite (Hem) and calcite (Cal).

Fig. 2: Typical transient signals for silica capillaries with internal diameter of 20 µm containing multi-element solutions at concentration of 10 µg g^{-1} (except Na with 1000 µg g^{-1}) analysed by LA-ICPQMS (a), LA-ICPSFMS (b) and LA-ICPTOFMS (c). Seven representative isotopes (^{7}Li, ^{23}Na, ^{29}Si, ^{65}Cu, ^{88}Sr, ^{139}La, ^{209}Bi) are shown here, but the dataset for all isotopes is given in Table 2. For QMS and SFMS, 35 isotopes were measured, whereas all isotopes are measured with the TOFMS (see Table 1). Signal duration (based on ^{23}Na), number of cycles and cycle times for each setup are indicated. Analytical conditions for the three setups are given in Table 1.

Fig. 3: Standard deviation versus mean concentration (n=4 to 7) for five selected isotopes (^{7}Li, ^{65}Cu, ^{88}Sr, ^{139}La, ^{209}Bi) from silica capillaries with internal diameter of 20 µm containing four different multi-element solutions at concentration of 0.1, 1, 10 and 50 µg g^{-1} (except for ^{23}Na with 1000 µg g^{-1}) analysed by LA-ICPQMS, LA-ICPSFMS and LA-ICPTOFMS. The precision is represented by the RSD (relative standard deviation). Dataset for all measured isotopes is given in Table 2. Elements with concentration below limit of detection are not represented. Analytical conditions for the three setups are given in Table 1.

Fig. 4: Mean and standard deviation (1σ) of concentrations measured by LA-ICPMS (LA-ICPQMS, LA-ICPSFMS and LA-ICPTOFMS) versus nominal concentration in standard solution for five selected isotopes (^{7}Li, ^{65}Cu, ^{88}Sr, ^{139}La, ^{209}Bi) from silica capillaries with internal diameter of 20 µm containing multi-element solutions. The accuracy is a function of the length of the orthogonal projection of the data points on the 1:1 slope. Circles and error bars stand for mean (n=4 to 7) and standard deviation (1σ) values respectively (see Table 2). Dataset for all measured isotopes is given in Table 2. Analytical conditions for the three setups are given in Table 1.

Fig. 5: Mean value for limits of detection (LOD) calculated for silica capillaries with internal diameter of 20 µm containing multi-element solutions at concentration of 10 µg g^{-1}, and analysed by LA-ICPQMS, LA-ICPSFMS and LA-ICPTOFMS. Analytical conditions for the three setups are given in Table 1.

Fig. 6: Typical transient signals for 25 µm two-phase fluid inclusions (sample BP-66-210, Alps) analysed by LA-ICPQMS (a), LA-ICPSFMS (b) and LA-ICPTOFMS (c). Corresponding signal/background ratios of analysed isotopes normalised to ^{23}Na (internal standard) are presented for LA-ICPQMS (d), LA-ICPSFMS (e) and LA-ICPTOFMS (f). Nine selected isotopes (^{7}Li, ^{11}B, ^{23}Na, ^{29}Si, ^{35}Cl, ^{85}Rb, ^{88}Sr, ^{121}Sb, ^{133}Cs) are shown here, but the dataset for all isotopes is given in Table 2.Analytical conditions for the three setups are given in Table 1.

Fig. 7: Total signal duration (a) and number of acquisition cycles (b) as function of fluid inclusion diameter for individual two-phase fluid inclusions measurement (sample BP-66-210, Alps) analysed by LA-ICPQMS, LA-ICPSFMS and LA-ICPTOFMS. The number of acquisition cycles is function of the cycle time for each configuration of LA-ICPMS (273 ms for QMS, 560 ms for SFMS and 30 ms for TOFMS). Analytical conditions for the three setups are given in Table 1. n: number of fluid inclusions analysed.

Fig. 8: Composition of two-phase fluid inclusions (sample BP-66-210, Alps) with different diameters (< 10 µm, 10-25 µm, > 25 µm) analysed by LA-ICPQMS (a), LA-ICPSFMS (b) and LA-ICPTOFMS (c). Dataset for all fluid inclusions is given in Table 3. Analytical conditions for the three setups are given in Table 1. n= number of fluid inclusions analysed.

Fig. 9: Typical transient signals for 5 μm two-phase fluid inclusions (sample BP-66-210, Alps) analysed by LA-ICPQMS (a) and LA-ICPTOFMS (b).

Fig. 10: Representation of different integration windows for a transient LA-ICPTOFMS signal from a 25 μm fluid inclusion (sample BP-66-210, Alps). (a) Na signal/background ratio as a function of time for 90, 95 and 100% of the total fluid inclusion Na signal. (b) Signal/background ratios for different isotopes as a function of Na signal/background ratio.

Fig. 11: Limits of detection (LODs) for LA-ICPQMS, LA-ICPSFMS and LA-ICPTOFMS as a function of two-phase fluid inclusion diameter (sample BP-66-210, Alps) for ^{11}B (a), ^{85}Rb (b), ^{133}Cs (c) and ^{208}Pb (d). The values are reported in Table 3. Analytical conditions for the three setups are given in Table 1. n= number of fluid inclusions analysed.

Fig. 12: Mean limits of detection (LODs) calculated for a series of individual fluid inclusions (sample BP-66-210, Alps) of diameter < 10 μm (a), 10-25 μm (b) and > 25 μm (c), analysed by LA-ICPQMS, LA-ICPSFMS and LA-ICPTOFMS. The values are reported in Table 3. Analytical conditions for the three setups are given in Table 1.

Fig. 13: Typical transient signals for 15 μm multi-phase fluid inclusions (sample 7703-25, Zambia) analysed by LA-ICPQMS and LA-ICPTOFMS. The signals for detected elements obtained by QMS with the standard ablation cell have all the same shape and are correlated in time (top left to middle left), as observed by constant ratios normalised to Na (bottom left). The signals obtained by TOFMS with the fast washout cell differ from one group of isotopes to another, as shown by variable ratios normalised to Na (bottom right), allowing to distinguish the signals of the aqueous phase, halite (Hl) and magnesium hydroxides (Hyd) (top right), and hematite (Hem) and uraninite crystals (Urn) (middle right). Analytical conditions for the three setups are given in Table 1.

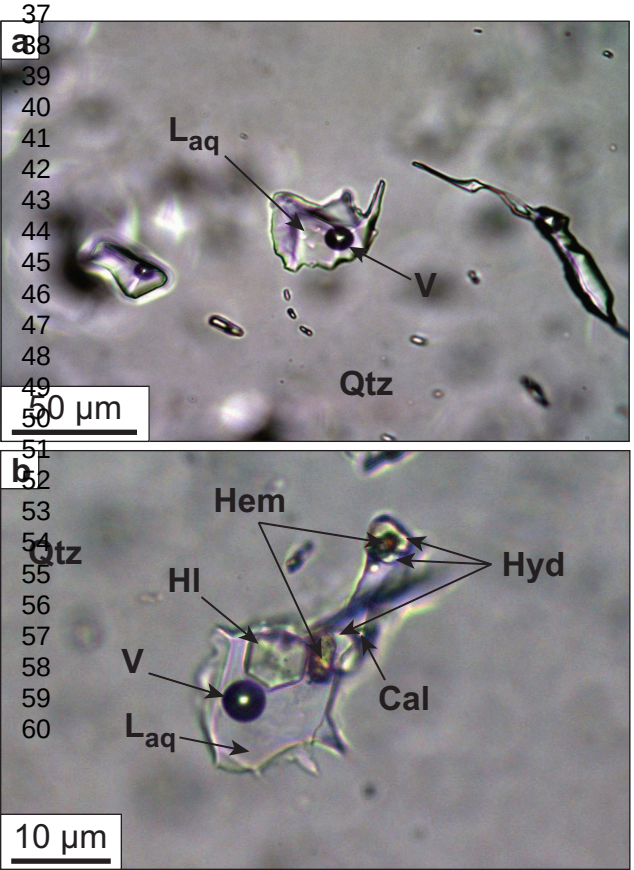

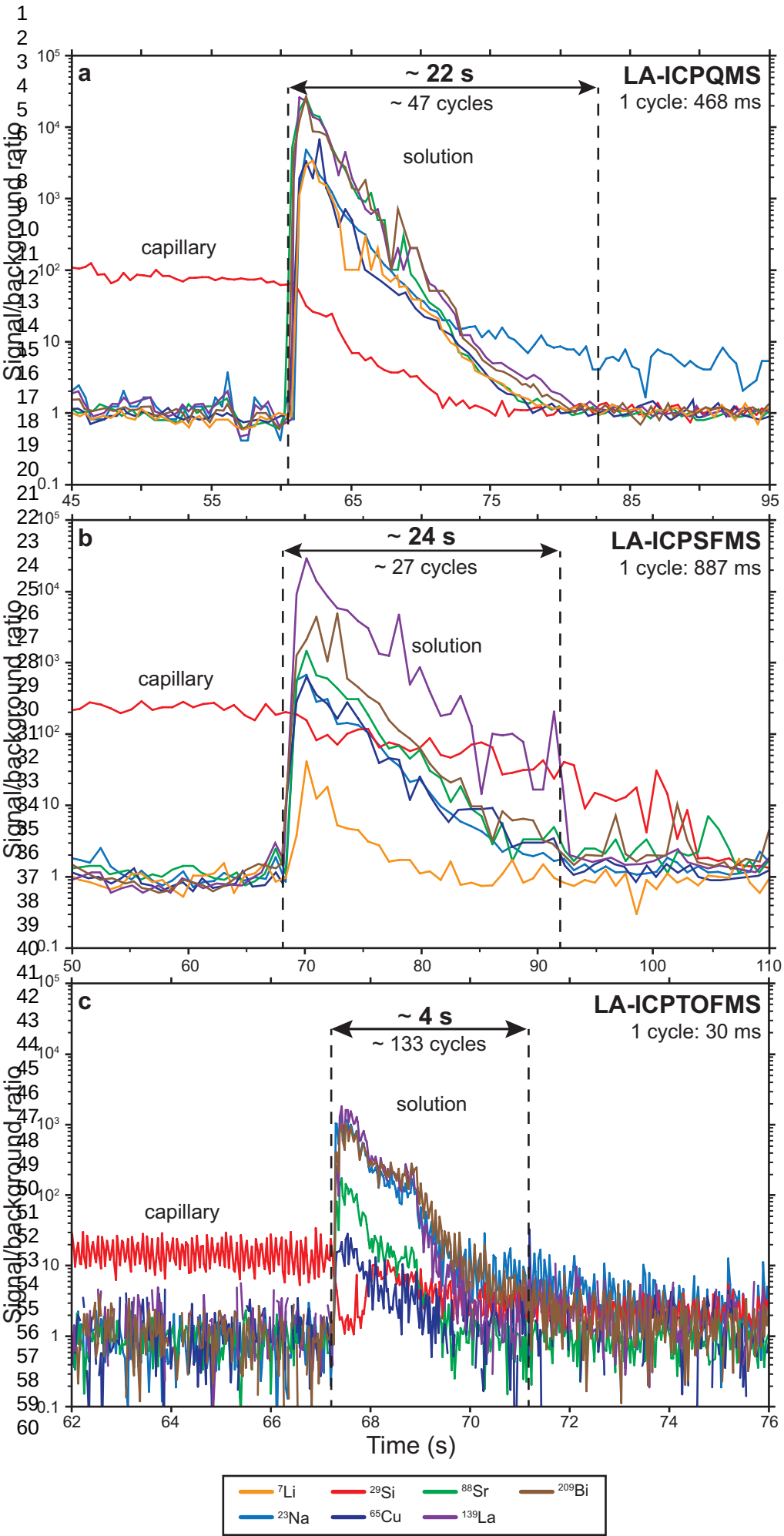

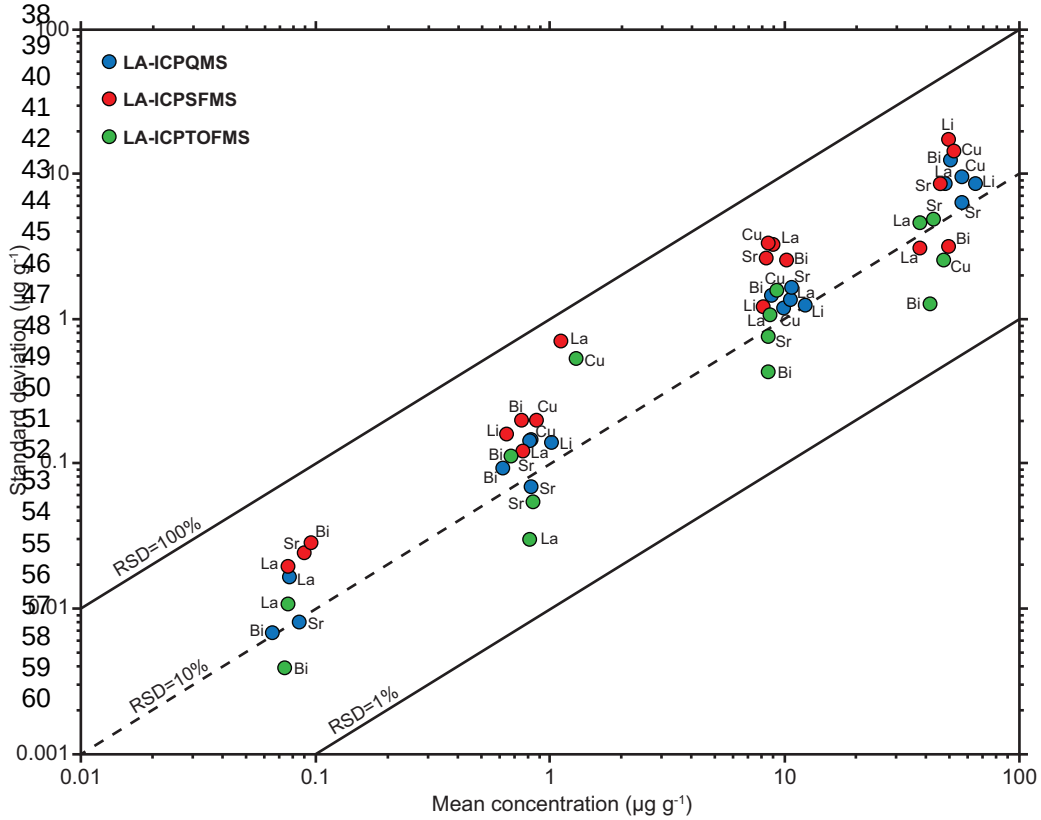

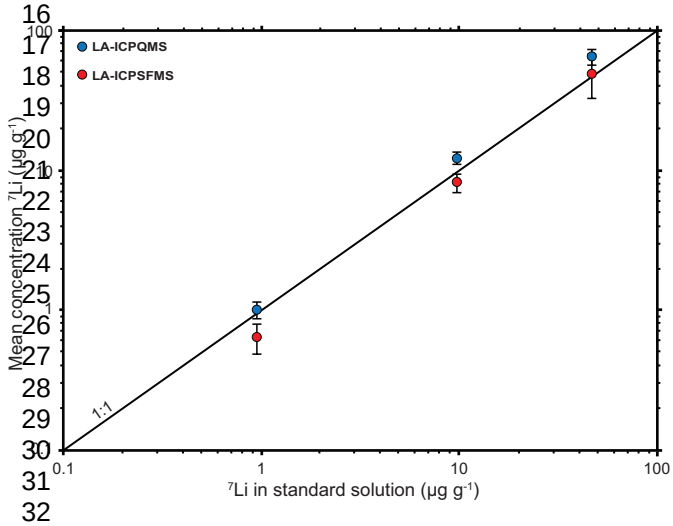

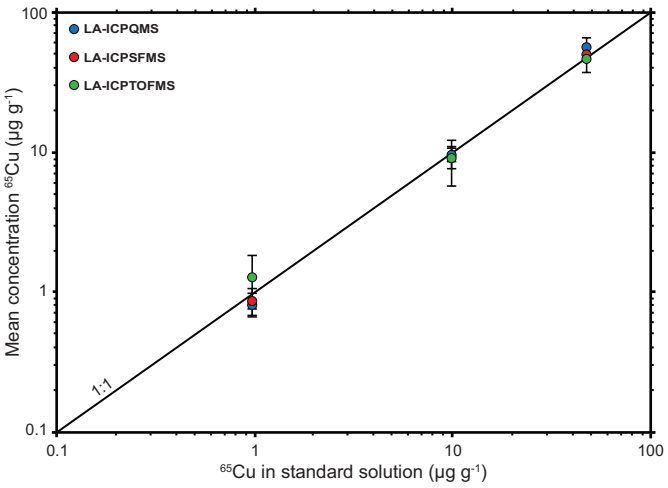

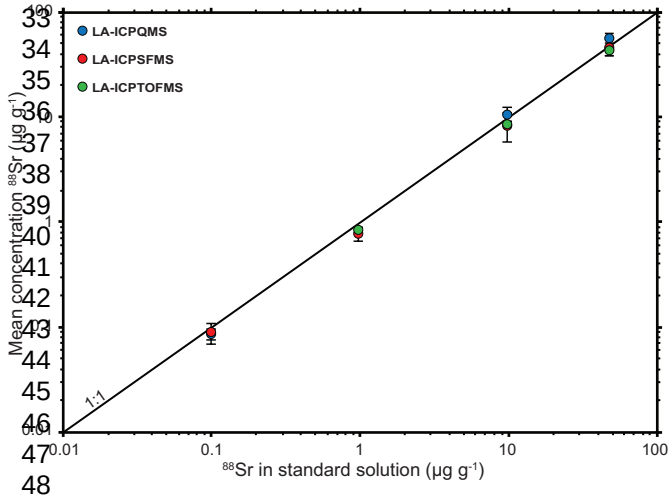

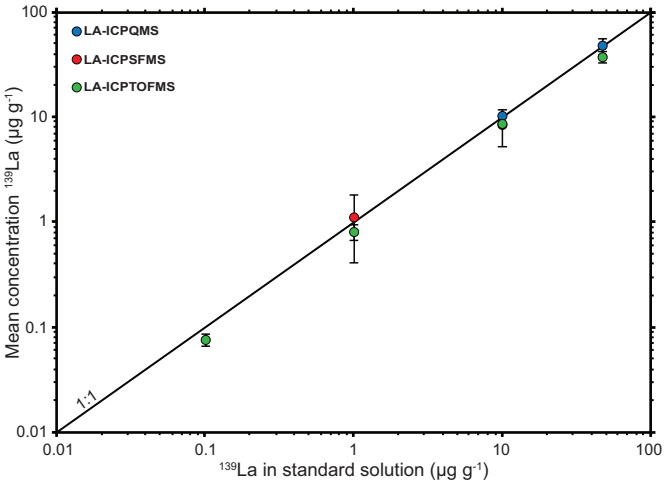

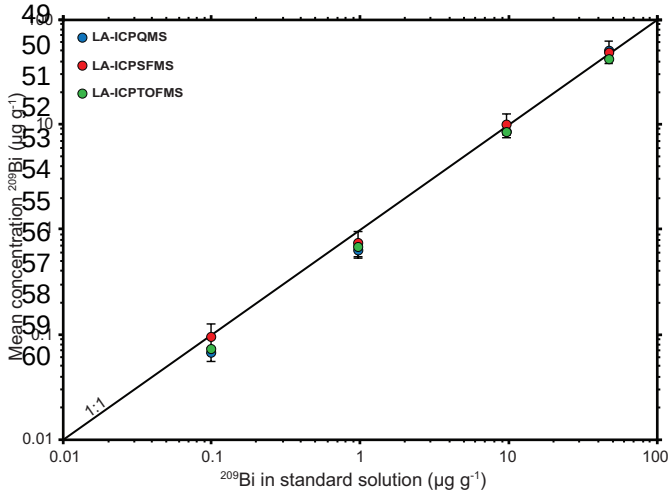

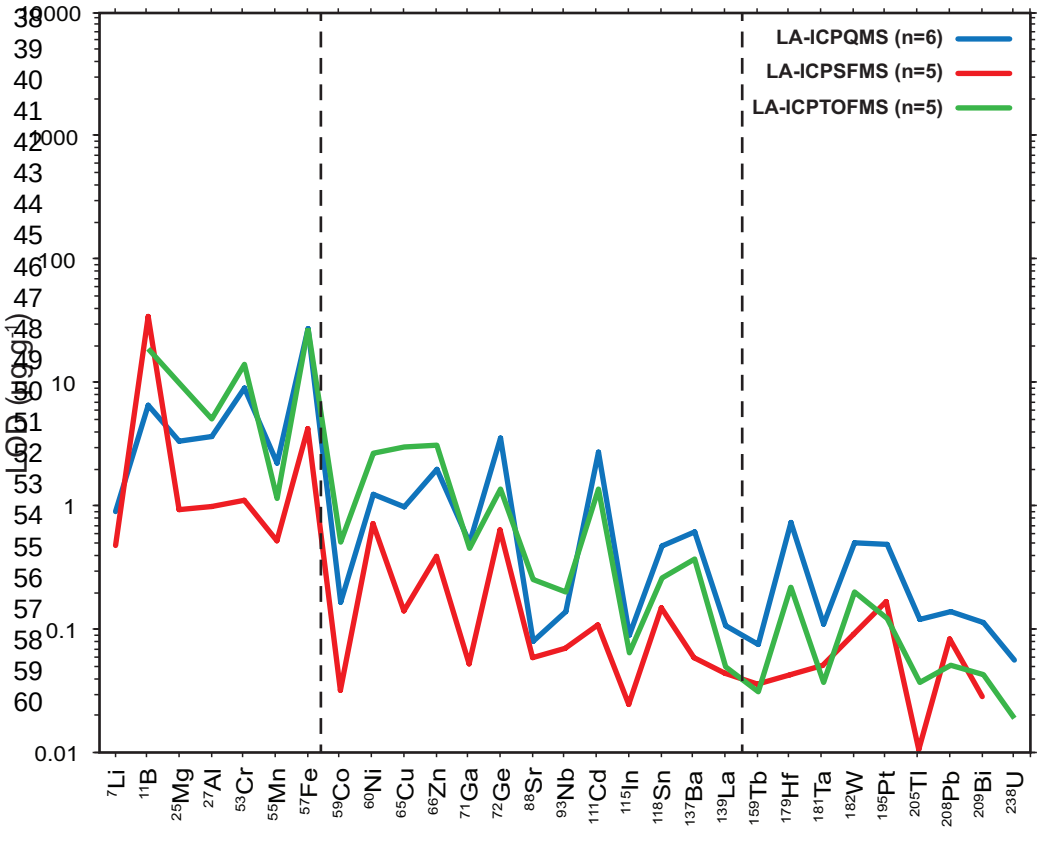

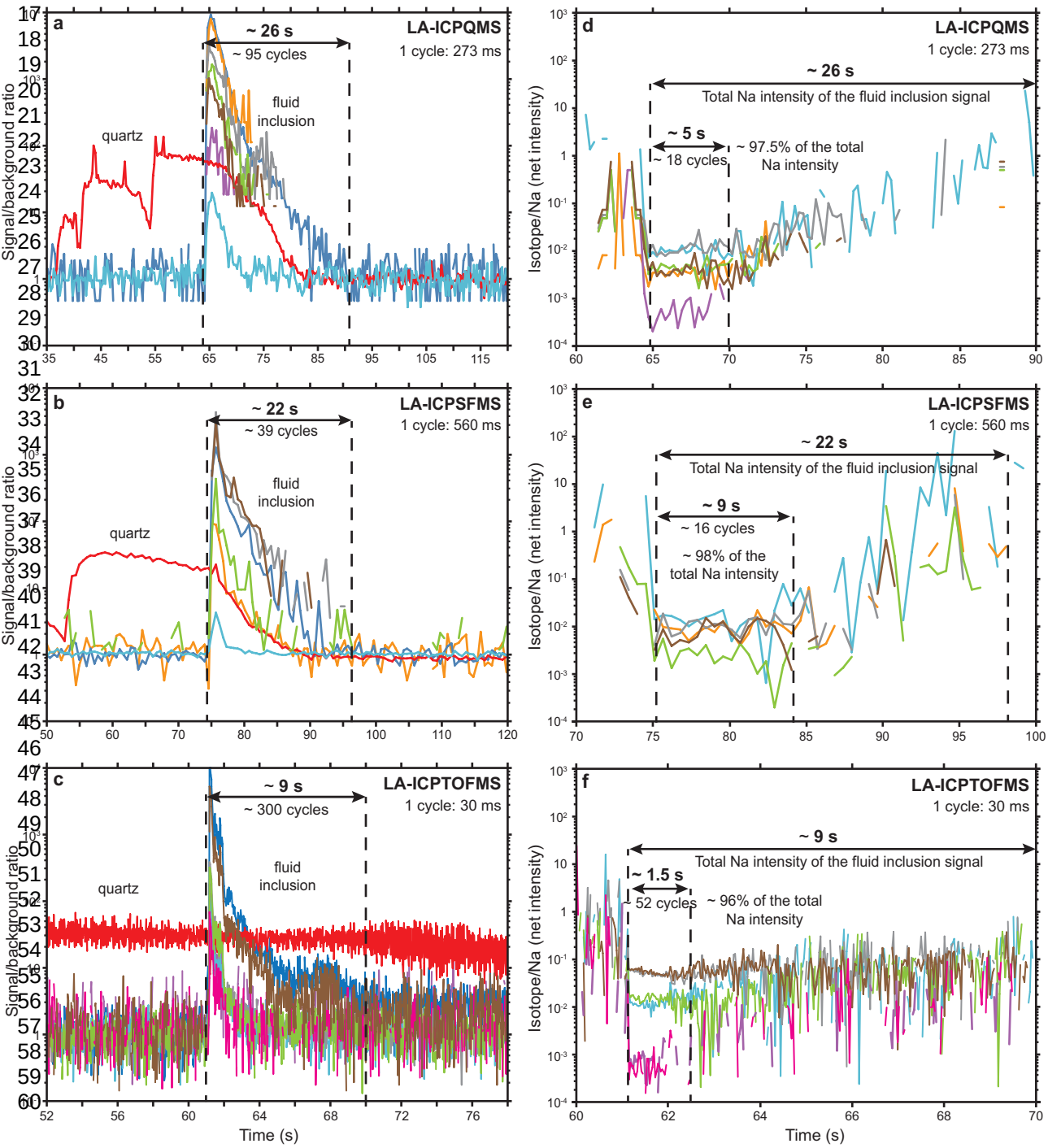

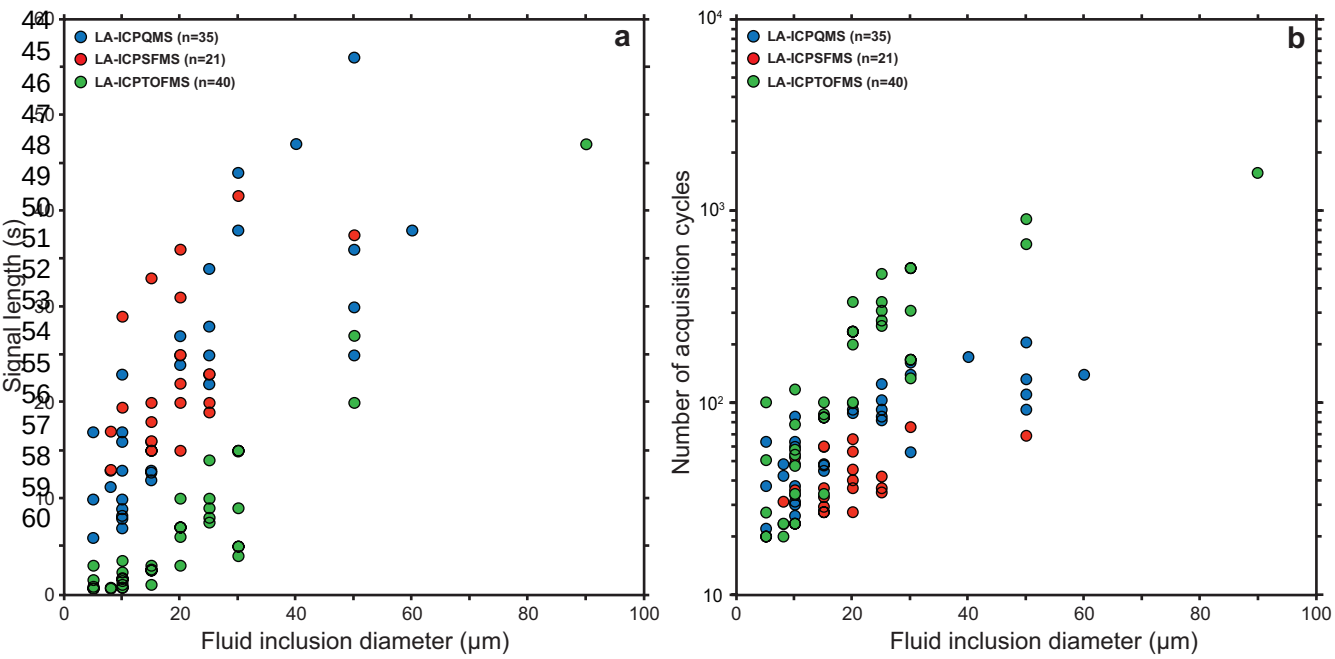

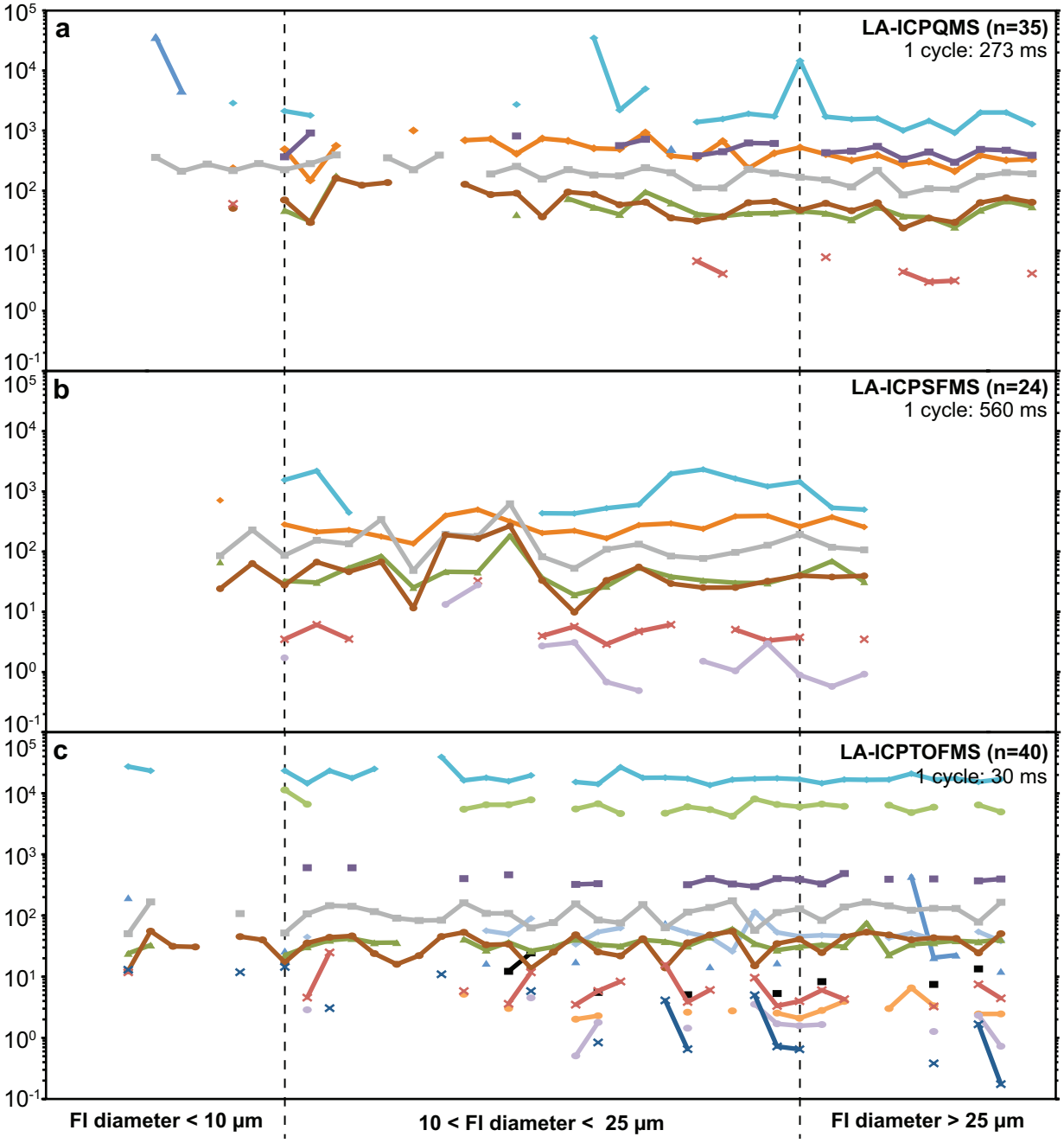

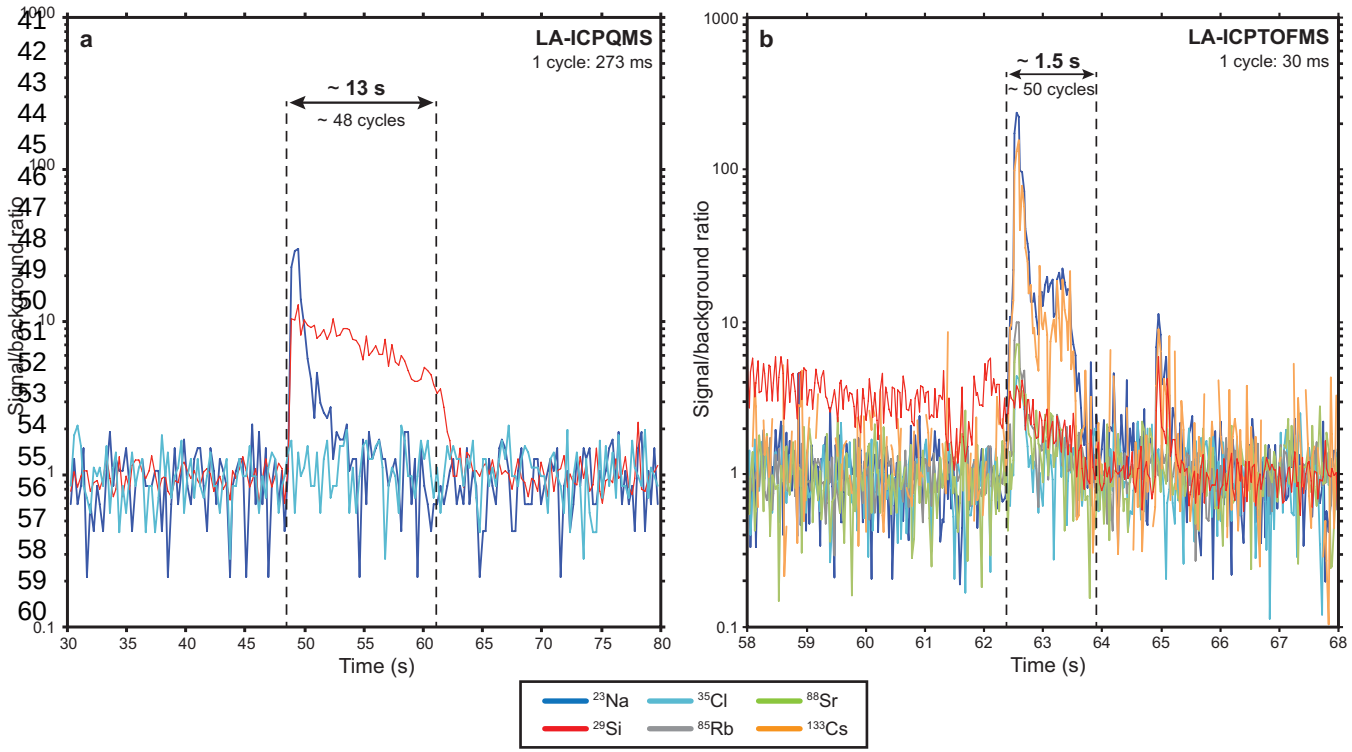

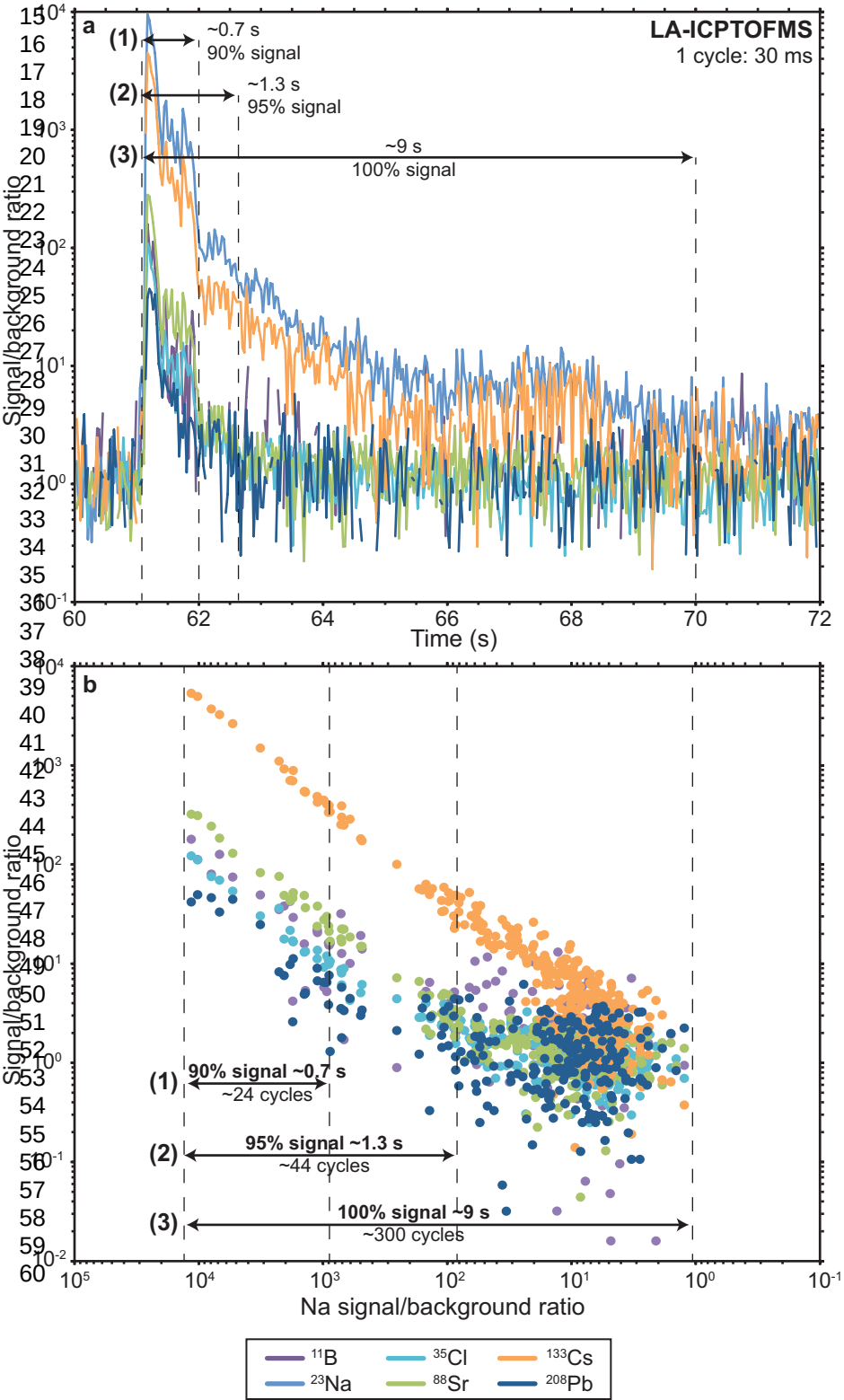

	LA-ICPQMS	LA-ICPSFMS	LA-ICPTOFMS
Model	Elan DRC Plus (PerkinElmer Inc.)	Element 2 (ThermoScientific)	Prototype (Tofwerk AG)
Laser	GeoLas ArF Excimer 193 nm (MicroLas)		
Ablation cell	Standard cylindrical cell		Fast washout tube cell
ICP-MS			
Plasma RF power	1380 W	1280 W	1300 W
Cooling gas (Ar)	17.5 L min^{-1}	16 L min^{-1}	16.5 L min^{-1}
Carrier gas (He)	1.2 L min^{-1}	1.1 L min^{-1}	0.6 L min^{-1}
Nebulizer gas (Ar)	0.72 L min^{-1}	0.84 L min^{-1}	1.2 L min^{-1}
Auxiliary gas (Ar)	0.8 L min^{-1}	0.66 L min^{-1}	1.2 L min^{-1}
Intensities (cps) on NIST SRM 610 for a low, mid and heavy isotope			
^{23}Na	1.6×10^7	1.2×10^8	5.3×10^5
^{140}Ce	1.5×10^5	1.7×10^6	4.7×10^4
^{209}Bi	1.0×10^5	1.7×10^6	7.0×10^4
Acquisition parameters for multi-element solutions in silica capillaries			
Cycle time	468 ms	887 ms	30 ms
Isotopes measured	^7Li, ^{11}B, ^{22}Ne, ^{23}Na, ^{25}Mg, ^{27}Al, ^{29}Si, ^{53}Cr, ^{55}Mn, ^{57}Fe, ^{59}Co, ^{60}Ni, ^{65}Cu, ^{66}Zn, ^{71}Ga, ^{72}Ge, ^{85}Rb, ^{88}Sr, ^{93}Nb, ^{111}Cd, ^{115}In, ^{118}Sn, ^{121}Sb, ^{133}Cs, ^{137}Ba, ^{139}La, ^{140}Ce, ^{159}Tb, ^{179}Hf, ^{181}Ta, ^{182}W, ^{195}Pt, ^{205}Tl, ^{208}Pb, ^{209}Bi, ^{238}U (U not measured with SFMS)		^6Li to ^{238}U
Acquisition parameters for two-phase fluid inclusions (sample BP-66-210, Alps)			
Cycle time	273 ms	560 ms	30 ms
Isotopes measured	^7Li, ^{11}B, ^{22}Ne, ^{23}Na, ^{25}Mg, ^{29}Si, ^{35}Cl, ^{44}Ca, ^{57}Fe, ^{59}Co, ^{65}Cu, ^{66}Zn, ^{79}Br, ^{85}Rb, ^{88}Sr, ^{133}Cs, ^{137}Ba, ^{140}Ce, ^{182}W, ^{197}Au, ^{208}Pb		^6Li to ^{238}U
Acquisition parameters for multi-phase fluid inclusions (sample 7703-25, Zambia)			
Cycle time	195 ms		30 ms
Isotopes measured	^{23}Na, ^{25}Mg, ^{29}Si, ^{34}S, ^{39}K, ^{44}Ca, ^{47}Ti, ^{57}Fe, ^{65}Cu, ^{85}Rb, ^{88}Sr, ^{95}Mo, ^{137}Ba, ^{208}Pb, ^{238}U		^6Li to ^{238}U

Concentration at ca. 50 pg g^{-1}

Isotopes	Solution Concentration	LA-ICPQMS Mean (n=5)	SD	LOD	Precision	Accuracy	LA-ICPSFMS Mean (n=6)	SD	LOD	Precision	Accuracy	LA-ICPTOFMS Mean (n=7)	SD	LOD	Precision	Accuracy
	ng g^{-1}	ng g^{-1}	ng g^{-1}	ng g^{-1}	%	%	ng g^{-1}	ng g^{-1}	ng g^{-1}	%	%	ng g^{-1}	ng g^{-1}	ng g^{-1}	%	%
^{7}Li	46.9	64.7	8.6	0.6	13	38	49.5	17.2	1	35	6	n.m.	n.m.			
^{11}B	47.7	59.1	23.1	4	39	24	< LOD		130			41.8	4.0	2	9	-12
^{25}Mg	47.5	48.1	5.6	1	7	1	40.8	7.7	2	19	-14	31.9	2.8	1	9	-33
^{27}Al	46.7	47.2	4.1	2	9	1	53.6	14.9	3	28	15	46.5	6.8	0.4	15	-0.5
^{52}Cr	47.3	51.9	5.7	5	11	10	48.8	13.1	3	27	3	44.0	1.6	1	4	-7
^{55}Mn	47.5	53.5	7.5	1	14	13	47.0	7.6	1	16	-1	47.3	2.4	0.1	5	-0.4
^{57}Fe	47.1	58.6	15.3	16	26	24	49.7	12.2	9	24	5	54.1	10.1	2.5	19	15
^{59}Co	46.8	58.0	3.8	0.2	7	24	42.4	5.4	0.1	13	-9	45.8	1.3	0.05	3	-2
^{60}Ni	47.4	58.8	8.8	0.9	15	24	49.2	11.7	2	24	4	47.2	2.0	0.3	4	-0.5
^{63}Cu	47.4	57.0	9.4	0.7	17	20	52.0	14.4	0.3	28	10	47.4	2.5	0.3	5	0
^{66}Zn	47.0	51.1	10.5	1.2	21	9	47.0	11.4	1	24	0.1	40.5	2.3	0.3	6	-14
^{71}Ga	47.1	51.2	9.1	0.4	18	9	43.3	7.4	0.2	17	-8	41.3	2.3	0.04	6	-12
^{72}Ge	47.4	49.9	9.2	2	18	5	47.5	12.3	2	26	0.1	41.0	2.5	0.3	6	-13
^{88}Sr	47.4	56.9	6.4	0.04	11	20	46.3	8.5	0.1	18	-2	43.1	4.9	0.03	11	-9
^{93}Nb	47.5	50.1	5.8	0.06	12	6	42.2	8.3	0.1	20	-11	41.5	5.1	0.02	12	-13
^{111}Cd	47.3	48.5	13.0	1.5	27	3	49.2	7.1	0.3	14	4	41.5	2.6	0.15	6	-12
^{115}In	47.5	54.2	15.3	0.05	28	14	46.8	5.6	0.06	12	-1	44.7	1.4	0.01	3	-6
^{118}Sn	47.5	49.3	8.8	0.2	18	4	42.7	8.6	0.3	20	-10	42.2	1.7	0.03	4	-11
^{137}Ba	47.2	109.6	11.3	0.4	10	132	92.2	13.7	0.1	15	95	86.8	10.2	0.04	12	84
^{139}La	47.8	47.9	8.5	0.07	18	0	37.9	3.1	0.04	8	-21	37.5	4.6	0.004	12	-21
^{140}Ce	47.2	53.0	5.1	0.05	10	12	38.2	4.2	0.05	11	-19	39.0	4.7	0.003	12	-17
^{178}Hf	47.2	51.7	7.1	0.3	14	10	43.3	10.0	0.09	23	-8	38.9	5.6	0.02	14	-17
^{180}Ta	47.3	21.2	4.2	0.05	20	-55	19.2	2.8	0.05	15	-59	13.5	4.0	0.004	30	-72
^{182}W	47.5	51.9	7.6	0.4	15	9	48.7	11.5	0.09	24	3	37.9	5.7	0.02	15	-20
^{195}Pt	47.5	55.0	22.9	0.5	42	16	48.6	14.1	0.4	29	2	20.0	4.8	0.01	24	-58
^{205}Tl	47.4	48.6	32.6	0.07	67	2	37.0	12.9	0.01	35	-22	19.6	3.4	0.005	17	-59
^{208}Pb	47.6	57.5	18.4	0.1	32	21	52.2	7.4	0.2	14	10	45.2	1.1	0.01	3	-5
^{209}Bi	47.3	50.6	12.4	0.06	25	7	49.4	3.1	0.05	6	4	41.7	1.3	0.01	3	-12
^{238}U	46.6	52.6	6.3	0.03	12	13	n.m.	n.m.				46.8	1.8	0.003	4	0.4

Concentration at ca. 10 pg g^{-1}

Isotopes	Solution Concentration	LA-ICPQMS Mean (n=6)	SD	LOD	Precision	Accuracy	LA-ICPSFMS Mean (n=5)	SD	LOD	Precision	Accuracy	LA-ICPTOFMS Mean (n=5)	SD	LOD	Precision	Accuracy
	ng g^{-1}	ng g^{-1}	ng g^{-1}	ng g^{-1}	%	%	ng g^{-1}	ng g^{-1}	ng g^{-1}	%	%	ng g^{-1}	ng g^{-1}	ng g^{-1}	%	%
^{7}Li	9.7	12.2	1.2	0.9	10	26	8.1	1.2	0.5	15	-16	n.m.	n.m.			
^{11}B	9.9	13.9	4.3	7	31	40	< LOD		35			< LOD		19		
^{25}Mg	9.9	10.4	1.7	3	16	6	11.0	5.3	0.9	49	11	8.7	1.0	10	11	-11
^{27}Al	9.7	9.2	2.6	4	29	-5	10.2	2.3	1.0	23	5	12.9	2.1	5	17	33
^{52}Cr	9.8	17.1	10.4	9	61	74	9.8	3.1	1	31	-0.5	< LOD		14		
^{55}Mn	9.9	10.2	1.2	2	11	4	9.0	2.3	0.5	25	-8	9.1	0.8	1	8	-8
^{57}Fe	9.8	26.5	9.4	27	35	170	17.4	8.3	4	48	77	< LOD		27		
^{59}Co	9.7	9.9	1.4	0.2	15	2	9.0	2.5	0.03	28	-7	8.7	0.4	0.5	5	-11
^{60}Ni	9.9	11.4	2.6	1	23	16	12.5	6.2	0.7	49	27	10.2	1.4	3	14	4
^{63}Cu	9.9	9.9	1.2	1	12	0.2	9.0	3.2	0.1	36	-9	9.3	1.6	3	17	-6
^{66}Zn	9.8	5.7	1.7	2	30	-42	8.2	1.8	0.4	22	-16	6.7	0.3	3	5	-31
^{71}Ga	9.8	9.8	2.0	0.5	21	0	8.1	2.1	0.05	26	-17	8.3	0.5	0.5	6	-16
^{72}Ge	9.9	10.2	2.4	4	23	3	8.6	1.9	0.6	22	-13	10.2	1.8	1	18	4
^{88}Sr	9.9	10.8	1.6	0.1	15	9	8.4	2.6	0.06	31	-15	8.5	0.8	0.3	9	-14
^{93}Nb	9.9	10.5	2.0	0.1	19	7	8.7	3.5	0.07	40	-12	8.6	1.1	0.2	13	-13
^{111}Cd	9.8	5.8	1.4	3	24	-41	10.1	2.6	0.11	26	2	8.0	0.5	1	7	-18
^{115}In	9.9	9.2	1.7	0.1	18	-7	8.3	2.0	0.02	24	-16	8.9	0.3	0.1	3	-10
^{118}Sn	10.1	9.2	1.5	0.5	16	-9	7.3	1.6	0.15	21	-28	8.4	0.5	0.3	6	-17
^{137}Ba	9.9	10.3	1.9	0.6	18	6	9.8	6.4	0.06	65	-1	8.8	0.7	0.4	8	-11
^{139}La	10.2	10.5	1.4	0.1	13	3	8.5	3.3	0.04	39	-16	8.6	1.1	0.05	12	-15
^{140}Ce	9.7	9.5	1.0	0.1	11	-2	8.1	2.1	0.04	26	-17	8.0	1.1	0.03	13	-18
^{178}Hf	9.8	10.0	1.0	0.7	10	2	8.4	2.0	0.04	24	-14	8.7	0.9	0.2	11	-11
^{180}Ta	9.8	6.6	0.7	0.1	10	-33	5.5	1.6	0.05	30	-44	5.3	0.8	0.04	16	-46
^{182}W	10.1	10.3	1.7	0.5	16	4	7.7	2.4	0.09	31	-24	9.1	0.7	0.2	8	-10
^{195}Pt	10.1	7.3	1.1	0.5	15	-28	6.5	1.2	0.17	19	-36	4.5	0.6	0.1	13	-55
^{205}Tl	9.9	3.6	1.2	0.1	34	-63	2.5	1.1	0.01	42	-74	2.9	0.4	0.04	13	-70
^{208}Pb	9.9	9.9	1.6	0.1	16	0.4	9.8	3.4	0.08	35	-1	9.1	0.3	0.05	3	-8
^{209}Bi	9.8	8.8	1.4	0.1	16	-11	10.1	2.6	0.03	25	3	8.4	0.4	0.04	5	-14
^{238}U	10.0	10.7	0.5	0.1	5	7	n.m.	n.m.				8.8	0.6	0.02	7	-12

Concentration at ca. 1 pg g^{-1}

Isotopes	Solution Concentration	LA-ICPQMS Mean (n=5)	SD	LOD	Precision	Accuracy	LA-ICPSFMS Mean (n=5)	SD	LOD	Precision	Accuracy	LA-ICPTOFMS Mean (n=6)	SD	LOD	Precision	Accuracy
	ng g^{-1}	ng g^{-1}	ng g^{-1}	ng g^{-1}	%	%	ng g^{-1}	ng g^{-1}	ng g^{-1}	%	%	ng g^{-1}	ng g^{-1}	ng g^{-1}	%	%
^{7}Li	0.96	1.01	0.1	0.3	14	6	0.64	0.2	0.5	25	-33	n.m.	n.m.			
^{11}B	0.98	< LOD		2			< LOD		52			< LOD		7		
^{25}Mg	0.98	0.87	0.2	1	18	-11	< LOD		2			< LOD		3		
^{27}Al	0.96	< LOD		0.8			1.15	0.3	0.9	26	20	< LOD		2		
^{52}Cr	0.97	< LOD		2			1.78	0.5	1	29	84	< LOD		5		
^{55}Mn	0.98	0.84	0.1	0.5	15	-15	0.88	0.2	0.5	20	-10	1.07	0.3	0.4	26	9
^{57}Fe	0.97	< LOD		6			9.68	4.9	4	50		< LOD		9		
^{59}Co	0.96	0.81	0.1	0.06	13	-16	0.69	0.1	0.03	13	-29	0.84	0.1	0.2	8	-12
^{60}Ni	0.97	0.98	0.2	0.3	16	1	2.06	1.6	0.7	79	113	1.81	0.7	0.9	41	87
^{63}Cu	0.97	0.83	0.1	0.2	18	-14	0.87	0.2	0.1	23	-10	1.29	0.5	1	41	33
^{66}Zn	0.97	0.59	0.4	0.5	60	-39	0.78	0.3	0.3	40	-19	1.27	0.5	1	39	31
^{71}Ga	0.97	0.70	0.1	0.1	11	-28	0.63	0.1	0.1	18	-36	0.73	0.03	0.2	5	-24
^{72}Ge	0.97	0.87	0.2	0.8	23	-10	1.11	0.3	0.6	31	14	0.89	0.1	0.5	10	-9
^{88}Sr	0.97	0.82	0.1	0.02	8	-15	0.77	0.1	0.03	16	-21	0.84	0.1	0.08	6	-14
^{93}Nb	0.98	0.58	0.1	0.03	15	-41	0.51	0.1	0.02	21	-48	0.43	0.1	0.07	15	-56
^{111}Cd	0.97	0.82	0.5	0.4	60	-16	0.92	0.2	0.06	23	-6	0.71	0.1	0.5	14	-27
^{115}In	0.98	0.73	0.1	0.02	16	-25	0.68	0.1	0.01	13	-30	0.76	0.1	0.02	8	-23
^{118}Sn	1.00	0.42	0.1	0.1	17	-58	0.54	0.2	0.1	29	-46	0.41	0.04	0.1	10	-59
^{137}Ba	0.98	0.90	0.1	0.2	10	-9	0.86	0.1	0.05	15	-12	0.79	0.1	0.1	17	-19
^{139}La	1.00	0.81	0.1	0.02	18	-19	1.11	0.7	0.01	63	11	0.81	0.03	0.02	4	-19
^{140}Ce	0.96	0.78	0.1	0.02	14	-19	0.83	0.2	0.01	27	-14	0.74	0.04	0.01	5	-23
^{178}Hf	0.97	0.86	0.2	0.1	27	-12	0.80	0.2	0.01	23	-18	0.74	0.1	0.07	9	-24
^{180}Ta	0.97	0.62	0.2	0.03	33	-37	0.72	0.3	0.01	35	-26	0.46	0.1	0.01	17	-52
^{182}W	1.00	0.92	0.2	0.2	27	-8	0.74	0.1	0.01	19	-26	0.78	0.1	0.06	8	-22
^{195}Pt	1.00	0.91	0.2	0.2	20	-9	0.97	0.3	0.2	32	-3	0.62	0.03	0.04	5	-38
^{205}Tl	0.97	0.93	0.1	0.03	16	-4	0.78	0.3	0.01	33	-20	0.80	0.1	0.01	16	-17
^{208}Pb	0.98	0.70	0.1	0.03	10	-29	0.83	0.2	0.05	18	-16	0.79	0.1	0.02	13	-19
^{209}Bi	0.97	0.62	0.1	0.03	15	-36	0.75	0.2	0.01	26	-22	0.68	0.1	0.02	17	-29
^{238}U	0.99	0.82	0.1	0.01	14	-17	n.m.	n.m.				0.78	0.03	0.01	4	-21

Concentration at ca. 0.1 pg g^{-1}

Isotopes	Solution Concentration	LA-ICPQMS Mean (n=5)	SD	LOD	Precision	Accuracy	LA-ICPSFMS Mean (n=5)	SD	LOD	Precision	Accuracy	LA-ICPTOFMS Mean (n=6)	SD	LOD	Precision	Accuracy
	ng g^{-1}	ng g^{-1}	ng g^{-1}	ng g^{-1}	%	%	ng g^{-1}	ng g^{-1}	ng g^{-1}	%	%	ng g^{-1}	ng g^{-1}	ng g^{-1}	%	%
^{7}Li	0.10	< LOD		0.2			< LOD		0.7			n.m.	n.m.			
^{11}B	0.10	< LOD		1			< LOD		70			< LOD		6		
^{25}Mg	0.10	< LOD		0.6			0.9	0.9	0.8	104		< LOD		3		
^{27}Al	0.10	< LOD		0.7			1.7		1			< LOD		2		
^{52}Cr	0.10	< LOD		2			1.8	1.3	1	76		< LOD		5		
^{55}Mn	0.10	< LOD		0.4			< LOD		0.6			< LOD		0.4		
^{57}Fe	0.10	< LOD		5			12.8	14.0	5	125		< LOD		10		
^{59}Co	0.10	0.08	0.01	0.04	6	-18	0.09	0.03	0.05	30	-8	< LOD		0.2		
^{60}Ni	0.10	0.6	0.2	0.2	27		< LOD	0.4	0.8			< LOD		1		
^{63}Cu	0.10	< LOD		0.2			< LOD	0.1	0.2			< LOD		1		
^{66}Zn	0.10	< LOD		0.4			0.5	0.6	0.5	122		< LOD		1		
^{71}Ga	0.10	< LOD		0.1			0.12	0.1	0.06	73	23	< LOD		0.2		
^{72}Ge	0.10	< LOD		0.6			< LOD		0.7			< LOD		0.6		
^{88}Sr	0.10	0.09	0.01	0.01	9	-14	0.09	0.02	0.04	27	-11	< LOD		0.1		
^{93}Nb	0.10	0.04	0.01	0.02	26	-58	0.05	0.02	0.03	50	-52	< LOD		0.1		
^{111}Cd	0.10	< LOD		0.3			0.2	0.1	0.08	91	53	< LOD		0.6		
^{115}In	0.10	0.08	0.01	0.01	9	-21	0.08	0.04	0.02	51	-20	0.08	0.02	0.03	18	-16
^{118}Sn	0.10	0.13	0.1	0.08	113	26	0.15	0.2	0.1	122	47	< LOD		0.1		
^{137}Ba	0.10	0.103	0.02	0.08	19	3	0.104	0.04	0.08	37	4	< LOD		0.1		
^{139}La	0.10	0.08	0.02	0.01	22	-23	0.08	0.02	0.01	26	-24	0.08	0.01	0.02	14	-24
^{140}Ce	0.10	0.07	0.01	0.01	16	-28	0.07	0.01	0.02	16	-31	0.07	0.004	0.01	6	-30
^{178}Hf	0.10	< LOD		0.10			0.05	0.04	0.03	73	-48	0.06	0.01	0.1	17	-42
^{180}Ta	0.10	0.06	0.02	0.01	38	-39	0.06	0.03	0.02	58	-43	0.05	0.02	0.02	36	-53
^{182}W	0.10	< LOD		0.13			0.2	0.2	0.03	111	114	< LOD	0.00	0.08		
^{195}Pt	0.10	< LOD		0.10			0.2	0.2	0.2	84	97	0.06	0.01	0.06	19	-36
^{205}Tl	0.10	0.07	0.003	0.03	4	-26	0.098	0.04	0.01	40	-2	0.09	0.01	0.02	17	-12
^{208}Pb	0.10	0.14	0.12	0.03	88	39	0.14	0.04	0.06	29	43	0.08	0.01	0.02	14	-18
^{209}Bi	0.10	0.07	0.01	0.02	10	-34	0.096	0.03	0.02	29	-4	0.07	0.00	0.02	5	-26
^{238}U	0.10	0.08	0.02	0.004	23	-17	n.m.	n.m.				0.08	0.01	0.01	8	-23

LA-ICPQMS

Isotopes	All FI n=35			FI diameter < 10 µm n=5			10 µm < FI diameter < 25 µm n=21			FI diameter > 25 µm n=9		
	Mean concentration µg g^{-1}	SD µg g^{-1}	RSD %	Mean LOD µg g^{-1}	Range µg g^{-1}	RSD %	Mean LOD µg g^{-1}	Range µg g^{-1}	RSD %	Mean LOD µg g^{-1}	Range µg g^{-1}	RSD %
^{7}Li	470	210	45	930	43 - 1265	57	333	5 - 1550	126	12	2 - 50	133
^{11}B	520	170	33	10700	370 - 19000	63	4200	45 - 14000	117	47	14 - 140	84
^{25}Mg	13900	19600	141	3500	290 - 6600	70	1250	23 - 5250	116	34	4 - 130	120
^{35}Cl	4110	7640	186	105000	1750 - 155000	61	37000	120 - 165000	130	199	30 - 705	109
^{44}Ca	< LOD			375000	36500 - 530000	55	142000	3050 - 450000	110	5450	1200 - 17000	118
^{57}Fe	< LOD			31000	2100 - 50000	58	11000	185 - 44000	118	290	42 - 1200	122
^{59}Co	< LOD			300	24 - 430	54	100	1.5 - 350	116	3	0.5 - 8	100
^{65}Cu	< LOD			1150	100 - 1600	53	400	6 - 1550	120	10	2 - 40	125
^{66}Zn	< LOD			2600	130 - 4000	60	800	8 - 2800	123	24	3 - 115	147
^{85}Rb	210	80	38	150	9 - 270	62	60	0.8 - 190	116	2	0.2 - 7	144
^{88}Sr	55	30	55	150	4 - 260	65	42	0.6 - 210	134	1	0.1 - 5	147
^{133}Cs	70	35	50	110	8 - 180	59	36	0.3 - 130	124	1	0.1 - 2.5	109
^{137}Ba	10	20	200	1610	23 - 2500	63	670	3 - 2700	128	6	0.7 - 15	84
^{140}Ce	< LOD			125	3 - 220	63	36	0.8 - 160	121	1	0.1 - 5	150
^{182}W	< LOD			515	31 - 825	58	235	3.5 - 1040	123	5	1 - 13	91
^{197}Au	< LOD			615	36 - 990	62	240	2.5 - 1050	129	5	0.8 - 23	135
^{208}Pb	< LOD			220	14 - 345	58	85	1 - 375	135	1	0.3 - 5	123

LA-ICPSFMS

Isotopes	All FI n=24			FI diameter < 10 µm n=5			10 µm < FI diameter < 25 µm n=17			FI diameter > 25 µm n=2		
	Mean concentration µg g^{-1}	SD µg g^{-1}	RSD %	Mean LOD µg g^{-1}	Range µg g^{-1}	RSD %	Mean LOD µg g^{-1}	Range µg g^{-1}	RSD %	Mean LOD µg g^{-1}	Range µg g^{-1}	RSD %
^{7}Li	300	130	43	6100	290 - 18000	126	60	3 - 254	134	8.5	0.4 - 17	135
^{11}B	< LOD			1040000	51700 - 3000000	127	10000	337 - 42600	148	1200.0	62 - 2345	134
^{25}Mg	< LOD			18000	750 - 56100	132	164	6 - 700	139	27.0	1.2 - 54	135
^{35}Cl	1100	710	65	2050000	101700 - 5930000	128	15335	32 - 79000	173	60.0	3.5 - 115	133
^{44}Ca	1430	610	43	600000	31500 - 1570000	123	6350	163 - 29000	143	750	37 - 1460	134
^{57}Fe	< LOD			106000	4700 - 300000	126	913	23 - 4150	147	84	4.5 - 164	134
^{59}Co	< LOD			950	33 - 2725	127	6	0.2 - 36	160	0.7	0.03 - 1.4	136
^{65}Cu	< LOD			3420	200 - 10000	120	32	1 - 170	153	3	0.2 - 6	135
^{66}Zn	< LOD			7700	250 - 23110	127	67	2 - 314	156	8	0.3 - 17	137
^{85}Rb	155	127	82	480	15 - 1170	109	5	0.1 - 34	166	0.3	0.03 - 0.6	129
^{88}Sr	49	36	73	950	53 - 2160	115	9	0.3 - 36	142	0.9	0.05 - 1.8	133
^{133}Cs	62	65	105	250	12 - 740	126	3	0.1 - 15	153	0.3	0.01 - 0.6	138
^{137}Ba	6.5	8	123	1950	124 - 5000	123	10	0.8 - 40	140	1.1	0.01 - 2.2	141
^{140}Ce	< LOD			143	7 - 390	124	2	0.1 - 11	142	0.4	0.26 - 0.6	52
^{182}W	4.4	8	182	334	27 - 1270	186	4	0.3 - 22	174	0.2	0.02 - 0.4	129
^{197}Au	< LOD			2300	106 - 6000	118	22	0.4 - 110	165	0.9	0.05 - 1.7	134
^{208}Pb	2	0.2	10	540	25 - 1650	129	6	0.2 - 35	135	1.0	0.06 - 1.9	133

LA-ICPTOFMS

Isotopes	All FI n=40			FI diameter < 10 µm n=7			10 µm < FI diameter < 25 µm n=24			FI diameter > 25 µm n=9		
	Mean concentration µg g^{-1}	SD µg g^{-1}	RSD %	Mean LOD µg g^{-1}	Range µg g^{-1}	RSD %	Mean LOD µg g^{-1}	Range µg g^{-1}	RSD %	Mean LOD µg g^{-1}	Range µg g^{-1}	RSD %
^{7}Li	n.m.	n.m.										
^{11}B	400	90	23	3010	485 - 6040	68	443	38 - 1455	92	290	43 - 700	86
^{25}Mg	78	130	167	1935	43 - 4130	81	180	3 - 1000	163	24	3 - 58	86
^{35}Cl	19000	5140	27	68200	6210 - 136500	72	8130	490 - 33650	115	3384	490 - 8200	86
^{39}K	6225	1461	23	109547	4410 - 233270	84	11320	316 - 59770	153	2450	365 - 6120	86
^{44}Ca	< LOD			355730	91340 - 630000	56	65700	7400 - 184500	74	56500	8160 - 136700	84
^{55}Mn	10	7	66	327	24 - 660	77	35	1.8 - 155	124	13	1.9 - 32	85
^{57}Fe	< LOD			8250	618 - 17050	77	917	47 - 4000	125	350	48 - 890	88
^{59}Co	< LOD			137	11 - 290	76	16	0.8 - 67	122	6	0.8 - 15	86
^{65}Cu	< LOD			463	66 - 884	68	64	5 - 205	90	37	6 - 92	88
^{66}Zn	< LOD			771	77 - 1520	73	94	4 - 377	114	40	6 - 92	84
^{75}As	53	19	36	495	47 - 1035	76	70	3.4 - 263	113	25	4 - 58	84
^{85}Rb	113	37	33	155	11 - 311	76	17	0.9 - 77	129	6	1 - 15	85
^{88}Sr	36	10	28	81	6 - 162	75	9	0.4 - 41	130	3	0.5 - 8	87
^{121}Sb	3.1	1.2	39	68	5 - 135	76	8	0.1 - 31	120	3	0.4 - 8	86
^{133}Cs	35	13	37	12	1 - 24	77	1.3	0.1 - 5	120	0.5	0.1 - 1.3	85
^{137}Ba	7.4	5	72	109	10	73	12	0.6 - 55	123	5	0.7 - 11	86
^{140}Ce	< LOD			14	1 - 26	71	1.6	0.1 - 6	117	0.6	0.1 - 1.5	84
^{182}W	2	1	60	56	4 - 115	78	6	0.3 - 28	125	2.2	0.3 - 5	84
^{197}Au	< LOD			34	2.5 - 70	77	4.3	0.2 - 17	117	1.4	0.2 - 3.5	86
^{208}Pb	4.9	5	104	18	1.2 - 38	78	2.0	0.1 - 9	127	0.7	0.1 - 1.8	87

Isotopes	LA-Q-ICP-MS (n=35)								
	Mean µg g^{-1}	SD µg g^{-1}	Precision %	LOD (µg g^{-1}) < 15 µm		15 - 30 µm		> 30 µm	
				Mean (n=14)	Range	Mean (n=15)	Range	Mean (n=6)	Range
^{7}Li	470	210	45	750	35 - 1550	90	5 - 360	5	2 - 11
^{11}B	520	170	33	9000	207 - 19000	1115	0 - 4900	26	14 - 38
^{25}Mg	13900	19600	141	2700	140 - 6600	400	23 - 2100	15	4 - 33
^{35}Cl	4110	7640	186	84200	740 - 163000	8240	120 - 45700	92	30 - 190
^{44}Ca	< LOD			300000	18300 - 533000	46560	3050 - 257000	2085	1180 - 4000
^{57}Fe	< LOD			24600	1000 - 49300	2850	185 - 12400	125	42 - 260
^{59}Co	< LOD			222	9 - 430	29	2 - 165	1	0.5 - 3
^{65}Cu	< LOD			905	55 - 1600	101	6 - 480	4	2 - 6
^{66}Zn	< LOD			1900	50 - 4000	221	8 - 1300	9	3 - 20
^{79}Br	< LOD			46400	1300 - 81500	5350	220 - 26000	163	53 - 300
^{85}Rb	210	80	38	128	4 - 270	14	0.7 - 63	0.7	0.2 - 1.5
^{88}Sr	55	30	55	106	0 - 260	10	0.7 - 37	0.3	0 - 0.6
^{133}Cs	70	35	50	85	2 - 180	9	0.3 - 38	0.3	0.1 - 0.6
^{137}Ba	10	20	200	1420	24 - 2670	147	3 - 635	4	0.7 - 7
^{140}Ce	< LOD			88	3 - 217	10	0 - 59	0.3	0.1 - 0.6
^{182}W	< LOD			460	13 - 1050	71	4 - 333	2	1 - 4
^{197}Au	< LOD			516	0 - 1050	62	3 - 362	2	0.8 - 4
^{208}Pb	< LOD			187	5 - 375	19	0 - 112	0.8	0.3 - 1.5

LA-SF-ICP-MS (n=24)

Isotopes	Mean	SD	Precision	LOD (µg g^{-1})				
	µg g^{-1}	µg g^{-1}	%	< 15 µm		15 - 30 µm		> 30 µm
				Mean (n=7)	Range	Mean (n=16)	Range	Mean (n=1)
^{7}Li	300	130	43	4370	15 - 18000	63	3 - 254	0.4
^{11}B	< LOD			744000	2160 - 3000000	10350	337 - 42600	62
^{25}Mg	< LOD			13000	29 - 56000	173	6 - 700	1
^{35}Cl	1100	710	65	1500000	330 - 6000000	16250	32 - 79000	4
^{44}Ca	1430	610	43	427000	1555 - 1600000	6615	163 - 29000	38
^{57}Fe	< LOD			75500	134 - 300000	955	23 - 4200	4.5
^{59}Co	< LOD			680	1.3 - 2750	6	0.2 - 37	0.1
^{65}Cu	< LOD			2450	6 - 9750	33	1 - 171	0.2
^{66}Zn	< LOD			5500	15 - 23000	70	2 - 315	0.3
^{79}Br	< LOD			72000	238 - 295000	1027	43 - 4915	4
^{85}Rb	155	127	82	342	0.6 - 1170	6	0.1 - 34	0.1
^{88}Sr	49	36	73	680	2 - 2160	10	0.3 - 36	0.1
^{133}Cs	62	65	105	180	0.1 - 737	3	0.1 - 15	0.1
^{137}Ba	6.5	8	123	1400	1 - 5000	10	0 - 40	0
^{140}Ce	< LOD			97	0 - 387	2	0 - 8	0.3
^{182}W	4.4	8	182	224	0 - 1267	4	0 - 23	0.1
^{197}Au	< LOD			1640	2 - 6000	23	0.5 - 109	0.1
^{208}Pb	2	0.2	10	387	2 - 1650	7	0.3 - 35	0.1

	LA-TOF-ICP-MS (n=40)			
Isotopes	Mean	SD	Precision	LOD (µg g^{-1})

Isotopes	µg g^{-1}	µg g^{-1}	%	< 15 µm		15 - 30 µm		> 30 µm	
				Mean (n=15)	Range	Mean (n=22)	Range	Mean (n=3)	Range
^{7}Li	< LOD			141500	15000 - 570000	14500	1800 - 44000	10800.0	2030 - 27500
^{11}B	400	90	23	1840	243 - 6040	270	38 - 694	233.0	43 - 600
^{25}Mg	78	130	167	1150	22 - 4128	36	3 - 338	19.0	3 - 48
^{35}Cl	19000	5140	27	41150	3564 - 136500	3520	490 - 11570	2700.0	490 - 7000
^{44}Ca	< LOD			220000	30600 - 630000	52200	7400 - 136700	42050.0	8160 - 106000
^{57}Fe	< LOD			4930	319 - 17050	370	48 - 1450	270.0	48 - 690
^{59}Co	< LOD			82	6 - 280	7	0.8 - 23	5.0	0.9 - 12
^{65}Cu	< LOD			280	35 - 884	39	5 - 105	30.0	6 - 75
^{66}Zn	< LOD			466	40 - 1517	42	4 - 150	32.0	6 - 82
^{79}Br	< LOD			10450	1424 - 33000	640	50 - 3100	280.0	64 - 555
^{85}Rb	113	37	33	93	7 - 311	7	0.9 - 27	5.0	1 - 12
^{88}Sr	36	10	28	48	3 - 162	3	0.4 - 15	2.3	0.5 - 6
^{133}Cs	35	13	37	7	0.5 - 24	0.6	0.1 - 2	0.4	0.1 - 1
^{137}Ba	7.4	5		65	5 - 213	5	0.7 - 20	3.8	0.7 - 10
^{140}Ce	< LOD			8	0.6 - 25	0.7	0.1 - 2.5	0.5	0.1 - 1
^{182}W	2	1		34	2 - 115	2.5	0.3 - 10	1.8	0.4 - 5
^{197}Au	< LOD			20	1.5 - 70	2	0.2 - 12	1.2	0.2 - 3
^{208}Pb	4.9	5	104	11	0.8 - 38	0.8	0.1 - 4	0.5	0.1 - 1.5

	LA-ICPQMS (n=10)						LA-ICPTOFMS			
	Concentration			LOD			Concentration			LOD
Isotopes	Mean	SD	RSD	Mean	Range	RSD	Mean	SD	RSD	Mean
	µg g^{-1}	µg g^{-1}	%	µg g^{-1}	µg g^{-1}	%	µg g^{-1}	µg g^{-1}	%	µg g^{-1}
^{24}Mg	n.m.	n.m.					384	168	44	39
^{25}Mg	600	628	105	142	14 - 710	140	470	126	27	238
^{26}Mg	n.m.	n.m.					625	35	6	325
^{27}Al	n.m.	n.m.					518	117	23	87
^{34}S	< LOD			11400	1325 - 51300	125	< LOD			14410
^{35}Cl	n.m.	n.m.					60350	18800	31	6000
^{39}K	6090	7135	117	360	40 - 1500	115	7700	3578	46	3350
^{44}Ca	19670	14502	74	12600	1400 - 55300	122	< LOD			176000
^{47}Ti	55	37	68	123	15 - 470	112	< LOD			930
^{55}Mn	n.m.	n.m.					3750	1870	50	30
^{57}Fe	15300	6040	39	1015	115 - 4250	117	15000	5065	34	850
^{59}Co	n.m.	n.m.					22	10	47	12
^{64}Zn	n.m.	n.m.					313	295	94	52
^{65}Cu	1800	1459	81	40	5 - 200	138	2100	362	17	96
^{66}Zn	n.m.	n.m.					346	271	78	77
^{67}Zn	n.m.	n.m.					457	395	86	410
^{68}Zn	n.m.	n.m.					475	461	97	310
^{85}Rb	61	80	133	6	0.6 - 27	122	52	45	86	11
^{86}Sr	n.m.	n.m.					639	346	54	81
^{88}Sr	818	1259	154	3	0.4 - 12	122	510	360	70	6
^{95}Mo	16	13	79	32	4.5 - 150	128	33	23	71	26
^{96}Mo	n.m.	n.m.					20	12	61	17
^{97}Mo	n.m.	n.m.					18			36
^{98}Mo	n.m.	n.m.					16	4	24	14
^{130}Te	n.m.	n.m.					23			22
^{133}Cs	n.m.	n.m.					14	14	95	1.1
^{135}Ba	n.m.	n.m.					1128	569	50	18
^{136}Ba	n.m.	n.m.					1123	553	49	39
^{137}Ba	1700	2217	130	45	7 - 180	111	1143	570	50	10
^{138}Ba	n.m.	n.m.					1119	565	51	1.4
^{139}La	n.m.	n.m.					2.1	0.8	40	1.2
^{140}Ce	n.m.	n.m.					1.5	0.7	46	1.1
^{141}Pr	n.m.	n.m.					0.8	0.6	70	0.9
^{143}Nd	n.m.	n.m.					9			8.5

^{205}Tl	n.m.	n.m.					1	1	77	1.5
^{206}Pb	n.m.	n.m.					387	380	98	4.2
^{207}Pb	n.m.	n.m.					328	326	99	5.0
^{208}Pb	390	512	131	6	0.8 - 21	103	321	322	100	2.0
^{209}Bi	n.m.	n.m.					2.5	0.9	37	1.5
^{238}U	4	2	39	1.7	0.1 - 7	107	3.3	1.6	48	0.8

S (n=5)

Range	RSD
µg g^{-1}	%
10 - 76	75
54 - 510	83
74 - 660	78
20 - 170	78
3800 - 30000	76
1640 - 10650	71
900 - 6150	74
40200 - 350000	78
222 - 1900	80
7 - 60	76
220 - 1600	73
3 - 25	75
12 - 105	76
20 - 250	99
18 - 160	77
100 - 825	77
80 - 640	77
3 -21	71
22 - 150	71
2 -10	69
7 - 50	74
5 - 32	72
10 - 67	72
4 - 27	75
6 - 45	78
0.3 - 2	77
5 - 35	76
12 - 71	70
3 - 20	77
0.3 - 3	74
0.3 - 2	75
0.3 - 2	73
0.2 - 1.8	75
2 - 17	74

0.4 - 3	76
1.1 - 9	79
1.3 - 10	78
0.5 - 4	77
0.3 - 3	82
0.2 - 2	79